

Supporting Information

Mechanochemistry with Metallosupramolecular Polymers

Diederik W. R. Balkenende^{1#}, Souleymane Coulibaly^{1#}, Sandor Balog¹, Yoan C. Simon¹,

Gina L. Fiore¹ & Christoph Weder^{*1}

¹*Adolphe Merkle Institute, University of Fribourg, CH-1700, Fribourg, Switzerland*

[#]These authors contributed equally

Table of Contents:

1. Materials and methods.....	2
2. Synthesis of compounds.....	4
3. Experimental procedures.....	9
4. Supporting discussion.....	11
5. Supporting figures.....	13
6. Characterization of compounds.....	51
7. Mechanical properties.....	65
8. Supporting movie.....	66

1. Materials and methods

Materials. Poly(ethylene-*co*-butylene) (Krasol®) of a number-average molecular weight of 3100 g/mol was obtained from Cray Valley HSC and dried *in vacuo* at 50 °C overnight before use. Spectroscopic grade CHCl₃ was passed through a plug of dry, activated (Brockman I) basic alumina prior to use. Tetrahydrofuran was purified by passage through alumina columns. Anhydrous CH₃CN, europium perchlorate (Eu(ClO₄)₃, 50% aqueous solution), europium chloride hexahydrate (EuCl₃·6H₂O), chelidamic acid, and all other reagents were used as received. The 2,6-bis(1'-methylbenzimidazolyl)pyridine (Mebip) ligand, the 2,6-bis(1'-methylbenzimidazolyl)-4-(dodecyloxy)pyridine, the 2,6-bis(1'-methylbenzimidazolyl)-4-oxypyridine-poly(ethylene-*co*-butylene)-2,6-bis(1'-methylbenzimidazolyl)-4-oxypyridine (BKB) macromonomer with a number-average molecular weight, M_n , = 4400 g/mol, and the metallocupramolecular polymer [Zn(BKB)](NTf₂)₂ were synthesized as previously reported^{1,2}.

Methods. ¹H (300 and 360 MHz) and ¹³C (75 and 90 MHz) NMR spectra were recorded on a Bruker Advance III spectrometer in CDCl₃ or DMSO-*d*₆. ¹H NMR coupling constants are given in Hz. ¹H NMR spectra were referenced against the signal of residual CHCl₃ or DMSO at 7.26 or 2.50 ppm and ¹³C NMR spectra were referenced against the signal of CDCl₃ or DMSO-*d*₆ at 77.0 or 39.52 ppm. UV-Vis spectra were recorded on a Shimadzu UV-2401 PC spectrophotometer in CHCl₃/CH₃CN (9:1) or in CHCl₃ solutions and with thin films that were drop-cast from CHCl₃ (Figure S24). Temperature-dependent UV-vis spectra were recorded on a Jasco V-670 Spectrophotometer equipped with a Jasco ETCR-762 Temperature Controller. FT-IR spectra were recorded using dried powder/films on a Perkin Elmer Spectrum 65 spectrometer between 4000 - 600 cm⁻¹ with a resolution of 4 cm⁻¹ and 5 scans per sample. CHN elemental analysis was performed by the Laboratory for Mass Spectroscopy of the University of Berne and the Service d'analyses chimiques of the Ecole d'ingénieurs et d'architectes Fribourg. Molecular weights were determined by gel permeation chromatography (GPC) (THF, 40 °C, 1.0 mL/min) using multi-angle laser light scattering

¹Kumpfer, J. R.; Taylor, S. D.; Connick, W. B.; Rowan, S. J. *J. Mater. Chem.* **2012**, *22*, 14196.

²Burnworth, M.; Tang, L.; Kumpfer, J. R.; Duncan, A. J.; Beyer, F. L.; Fiore, G. L.; Rowan, S. J.; Weder, C. *Nature* **2011**, *472*, 334.

(MALLS) ($\lambda = 658 \text{ nm}$, $25 \text{ }^\circ\text{C}$) and refractive index ($\lambda = 658 \text{ nm}$, $40 \text{ }^\circ\text{C}$) detection. A Polymer Laboratories $5 \text{ }\mu\text{m}$ mixed-C guard column and two GPC columns along with Wyatt Technology Corp. (Optilab REX interferometric refractometer, miniDawn TREOS laser photometer) and Agilent Technologies instrumentation (series 1200 HPLC) and Wyatt Technology software (ASTRA) were used for the GPC analysis. The incremental refractive index (dn/dc) was estimated by a single-injection method that assumed 100% mass recovery from the columns. All ultrasonication experiments were performed with a Branson Model 450 ultrasonic 1/2 in horn sonicator with an attached 1/8 inch tapered microtip. The length of the sonication pulses was varied as specified, and unless otherwise specified the amplitude was set to 20%. Excitation and emission spectra were recorded on a PTI C720 fluorescence spectrometer using right angle excitation. A XeArc lamp was used for excitation and a PTI 814 photomultiplier detection system was used for all photoluminescence experiments, unless indicated otherwise. Temperature-dependent luminescence spectra were recorded on a Jasco V-630 Spectrophotometer equipped with a Jasco ETC-272T Temperature Controller. The measurements were performed varying the temperature from $25 \text{ }^\circ\text{C}$ to $53 \text{ }^\circ\text{C}$ by increments of $2 \text{ }^\circ\text{C}$ allowing for a 3 min equilibration between each step. Thermogravimetric analyses (TGA) were conducted under N_2 using a Mettler-Toledo STAR thermogravimetric analyzer in the range of $25 \text{ }^\circ\text{C}$ to $500 \text{ }^\circ\text{C}$ with a heating rate of $10 \text{ }^\circ\text{C}/\text{min}$. Differential scanning calorimetry (DSC) measurements were performed under N_2 using a Mettler-Toledo STAR system modulated differential scanning calorimeter operated in modulated mode (amplitude $\pm 1^\circ\text{C}$, period 60 s, heating/cooling rate $10 \text{ }^\circ\text{C}/\text{min}$, range -70 to $150 \text{ }^\circ\text{C}$). Data from the second heating cycle and the reverse heat flow curve are reported unless indicated otherwise (T_d = onset point of decomposition, T_g = glass transition temperature). Dynamic mechanical thermal analyses (DMTA) were conducted under N_2 on a TA Instruments DMA Q 800 with a heating rate of $3 \text{ }^\circ\text{C}/\text{min}$ and a frequency of 1 Hz in the range of $-70 \text{ }^\circ\text{C}$ to $150 \text{ }^\circ\text{C}$, unless indicated otherwise. The stress strain measurements were conducted at $25 \text{ }^\circ\text{C}$, with a strain rate of $5 \text{ } \%/ \text{min}$. All mechanical tests were conducted on dog-bone-shaped samples. Reported mechanical data are averages of 3-5 independent experiments and all errors are standard deviations. The tensile moduli were calculated from the slopes of the linear region in the

strain regime of 0 - 0.5 % strain. The area under the stress-strain curves was determined to quantify the toughness.

2. Synthesis of compounds

Synthesis of 4-hydroxy-pyridine-2,6-dicarboxylic acid diethyl ester. The product was synthesized according to a previously reported procedure.³ ¹H NMR (360 MHz, DMSO-*d*₆): δ = 7.47 (s, 2H), 5.75 (s, 1H), 4.32 (q, J = 14.2 Hz, 4H), 1.31 (t, J = 7.2 Hz, 6H). ¹³C NMR (90 MHz, DMSO-*d*₆): δ = 168.85, 165.08, 149.57, 116.60, 116.28, 61.58, 14.50, 14.42.

Synthesis of dipicolinate diethyl ester-poly(ethylene-co-butylene)-dipicolinate diethyl ester. A round bottom flask was charged with hydroxyl-terminated poly(ethylene-co-butylene) (M_n = 3,100 g/mol, 10.14 g, 3.4 mmol) and dried *in vacuo* at 50°C for 18 h. Under a N₂ atmosphere, 4-hydroxy-pyridine-2,6-dicarboxylic acid diethyl ester (2.43 g, 10.1 mmol), triphenyl phosphine (2.59 g, 20.3 mmol) and THF (25 mL) were subsequently added. The reaction mixture was cooled to 0 °C and diisopropylazodicarboxylate (DIAD, 4 mL, 20.3 mmol) was added dropwise. The reaction mixture was allowed to slowly warm to room temperature and stirred for 60 h. The solvent was subsequently removed *in vacuo* and the resulting orange oil was dissolved in hot hexanes (200 mL). The resulting solution was extracted with methanol (3 × 150 mL) and 1M NaOH (aq) (3 × 150 mL). The organic solvent was removed *in vacuo* and the resulting product was further purified by flash column chromatography (SiO₂, DCM:MeOH 100:0 → 90:10). The purified product was dried for 24 h *in vacuo* and obtained as a slightly yellow, transparent oil: 6.5 g; 1.8 mmol; 53%, 97% conversion of OH groups, as measured by end group analysis using a previously reported procedure.⁴ ¹H-NMR (CDCl₃, 300 MHz): δ = 7.79 (s, 3-*H*, 5-*H*), 4.49 (q, J = 7.1 Hz, CH₃), 4.16 (q, J = 6.8 Hz, 4H), 4.02 (s), 1.93 – 0.96 (m, 510H), 1.47 (t, J = 7.1 Hz, 7H), 0.84 (t, J = 6.8 Hz, 157H). Weak signals around 4.02 ppm originating from residual DIAD, and partial

³Chauvin, A.-S.; Comby, S.; Song, B.; Vandevyver, C. D. B.; Bünzli, J.-C. G. *Chem. Eur. J.* **2008**, *14*, 1726.

⁴Keizer, H. M.; van Kessel, R.; Sijbesma, R. P.; Meijer, E. W. *Polymer* **2003**, *44*, 5505.

deprotection of the carboxylic acid functions were observed. ^{13}C NMR (CDCl_3 , 91 MHz): δ = 167.09, 165.28, 164.77, 150.10, 149.75, 114.60, 114.49, 114.36, 62.38, 53.12, 39.10, 38.87, 38.40, 37.89, 36.12, 33.44, 33.24, 30.66, 30.21, 29.75, 26.78, 26.60, 26.44, 26.26, 26.13, 26.04, 25.88, 14.19, 10.88, 10.68, 10.64, 10.53, 10.35, 10.21. GPC (MALLS) M_n = 3500 g/mol; polydispersity index, PDI = 1.18.

Synthesis of dipicolinic acid-poly(ethylene-co-butylene)-dipicolinic acid (DKD). H_2O (2.5 mL) was added dropwise to a solution of dipicolinate diethyl ester-poly(ethylene-co-butylene)-dipicolinate diethyl ester (0.980 g, 0.14 mmol) and potassium hydroxide (0.650 g, 11.6 mmol) in THF (50 mL). After the addition was complete, the mixture was stirred at room temperature for 15 h and became heterogeneous as the reaction proceeded. The reaction mixture was finally diluted with H_2O (150 mL), and 1M HCl was added dropwise until a pH value of 4 was reached. The crude product was collected by vacuum filtration to afford an off-white, tacky solid. The product was purified by dissolving it in a minimum amount of CHCl_3 (15 mL) and trifluoroacetic acid (0.5 mL) and precipitating this solution into a cold MeOH/ H_2O mixture (0 °C, 80:20, 200 mL). The precipitate was collected by vacuum filtration and dried *in vacuo* 70 °C for 24 h to afford the product as a white, tacky solid (930 mg, 0.27 mmol, 98%). ^1H -NMR (CDCl_3/TFA , 30:1, 300 MHz): δ = 8.00 (s, 4H), 4.42 (s, 4H), 2.22 – 0.97 (m, 561H), 0.83 (t, J = 6.8 Hz, 180H). ^{13}C NMR (CDCl_3 , 75 MHz): δ = 77.16, 39.05, 36.29, 33.61, 33.41, 30.83, 30.38, 29.93, 26.95, 26.76, 26.61, 26.29, 26.21, 26.05, 11.02, 10.80, 10.70. IR (cm^{-1}) 2959, 2920, 2872, 2852, 1725, 1592, 1460, 1378, 1310, 1274, 1116, 1035, 884, 770, 721, 637. Anal. Calcd for DKD: C 81.50, H 12.69, N 0.82. Found: C 79.03, H 12.77, N 0.80.

Synthesis of diethyl 4-(dodecyloxy)pyridine-2,6-dicarboxylate. A round bottom flask was charged with 4-hydroxy-pyridine-2,6-dicarboxylic acid diethyl ester (1.00 g, 4.18 mmol), 1-bromo-dodecane (1.50 ml, 6.27 mmol), K_2CO_3 (1.73 g, 12.5 mmol) and dry DMF (50 mL) under a N_2 atmosphere. The heterogeneous reaction mixture was stirred at 90 °C for 15 h. The reaction mixture was then cooled to room temperature and the solids were filtered off.

The DMF was removed *in vacuo* and the crude product was dissolved in CHCl_3 and purified by flash column chromatography (SiO_2 , CHCl_3 :MeOH 100:0 \rightarrow 90:10). The organic fractions were concentrated *in vacuo* to afford a white, tacky solid: 0.88 g; 2.16 mmol; 52 %. Purity of the intermediate was confirmed by elemental analysis: Anal. Calcd. for $\text{C}_{23}\text{H}_{37}\text{NO}_5$: C 67.78, H 9.15, N 3.44. Found: C 67.6, H 9.2, N 3.5.

Synthesis of 4-(dodecyloxy)pyridine-2,6-dicarboxylic acid ($\text{dpaC}_{12}\text{H}_{25}$). A solution of KOH (0.34 g, 6.13 mmol) in H_2O (10 mL) was added to a solution of diethyl 4-(dodecyloxy)pyridine-2,6-dicarboxylate (0.25 g, 0.61 mmol) in THF (40 mL) and the mixture was stirred at room temperature for 15 h. The reaction mixture was subsequently poured into H_2O (100 mL) and the product precipitated as a powder. An aqueous HCl solution (1M) was added dropwise until a pH value of 4 was reached. The precipitate was collected by vacuum filtration and dried *in vacuo* for 24 h at 60 °C to afford the product as a white powder: 0.12 g; 0.34 mmol; 55 %. ^1H NMR (300 MHz, $\text{DMSO-}d_6$) δ 7.62 (s, 2H, Ph-*H*), 4.14 (t, $J = 6.4$ Hz, 2H, -O- CH_2 -(CH_2) $_{10}$ -), 1.77 – 1.55 (m, 2H, -O- CH_2 - CH_2 -), 1.45 – 1.30 (m, 2H, -O-(CH_2) $_2$ - CH_2 -), 1.22 (m, 20H, -(CH_2) $_{10}$ - CH_3), 0.78 (t, $J = 6.7$ Hz, 3H, - CH_2 - CH_3). ^{13}C NMR (75 MHz, $\text{DMSO-}d_6$) δ 166.73, 165.24, 149.69, 113.45, 68.67, 31.25, 28.98, 28.96, 28.90, 28.66, 28.58, 28.11, 25.19, 22.05, 13.91. IR (cm^{-1}) 3240, 2918, 2850, 1753, 1734, 1725, 1604, 1562, 1466, 1445, 1417, 1402, 1362, 12791, 1190, 1106, 1055, 1031, 1010, 907, 877, 754, 695, 681, 639, 614. Anal. Calcd for $\text{C}_{19}\text{H}_{29}\text{NO}_5$: C 64.93, H 8.32, N 3.99. Found: C 65.3, H 8.7, N 3.8.

Metallosupramolecular polymerization of $[\text{Eu}(\text{BKB})_{1.5}](\text{ClO}_4)_3$ and film formation. To ensure a proper 3:1 stoichiometric ratio of Mebip ligands to Eu^{3+} ions, a solution of BKB was first titrated with $\text{Eu}(\text{ClO}_4)_3$ according to a previously reported procedure². UV-vis absorption spectra were acquired upon titration of BKB (25 μM) in 9:1 CHCl_3 : CH_3CN (v/v) with $\text{Eu}(\text{ClO}_4)_3$. The absorbance at 347 nm, characteristic for the formation of the Eu^{3+} :BKB

complex, was plotted as a function of the Eu^{3+} : BKB ratio and the end point of the titration was determined from the intersection of the linear segments of the curve. The end point was assumed to occur at a Eu^{3+} :BKB ratio of 0.66 and this information was used to calculate the required amount of BKB (Figure S11).² A solution of $\text{Eu}(\text{ClO}_4)_3$ (250 μL , 0.31 M, 77 μmol) in CH_3CN was added to a solution of BKB (0.53 g, 0.12 mmol) in CHCl_3 (5 mL) and a rapid increase of the viscosity was observed. The mixture was stirred at room temperature for 20 min and was subsequently concentrated *in vacuo* to afford a white tacky solid. Colorless films with a thickness of 150-250 μm were prepared by compression-molding the product at 140 $^\circ\text{C}$ and a pressure of 3 tons for 10 min in a Carver[®] press. IR (cm^{-1}) 3309, 2959, 2921, 2872, 2852, 1719, 1606, 1566, 1491, 1460, 1407, 1379, 1330, 1312, 1243, 1187, 1093, 1026, 930, 866, 754, 747, 723, 622. Anal. Calcd for $[\text{Eu}(\text{BKB})_{1.5}](\text{ClO}_4)_3$: C 77.89, H 12.05, N 2.98. Found: C 78.01, H 12.38, N 2.87.

Metallosupramolecular polymerization of $[\text{Fe}(\text{BKB})_{1.0}](\text{ClO}_4)_2$ and film formation. A solution of $\text{Fe}(\text{ClO}_4)_2 \cdot 6\text{H}_2\text{O}$ (1.46 mL, 0.04 M, 0.06 mmol) in CH_3CN was added to a solution of BKB (0.26 g, 0.06 mmol) in CHCl_3 (3 mL) and a rapid increase of the viscosity was observed. The mixture was stirred at room temperature for 20 min and was then concentrated *in vacuo* to afford a dark purple solid. Films with a thickness of 180-200 μm were prepared by compression-molding the product at 120 $^\circ\text{C}$ and a pressure of 3 tons for 10 min in a Carver[®] press.

Metallosupramolecular polymerization of $[\text{Eu}(\text{DKD})_{1.5}](\text{NH}_4)_3$ and film formation. The macromonomer DKD, (500 mg, 0.14 mmol), triethylamine (820 μL , 5.6 mmol) and CHCl_3 (20 mL) were combined in a round bottom flask and the solution was ultrasonicated at 40 $^\circ\text{C}$ for 20 min in an ultrasonication bath (VWR ultrasonic cleaner, 45 kHz, 120 W). A solution of

EuCl₃·6H₂O (46.4 mg, 94 μmol) in ethanol (0.5 mL) was then added and the reaction mixture immediately became viscous. The reaction mixture was stirred for 1 h and then concentrated *in vacuo*. To remove excess triethylamine, CHCl₃ (3 × 15 mL) was added to the product and removed *in vacuo*. The purified product was dried *in vacuo* at 80 °C overnight to yield the polymer as an off-white solid. Colorless films with a thickness of 150-250 μm were prepared by compression-molding the product at 160 °C and a pressure of 4 tons for 20 min in a Carver[®] press.

***In situ* preparation of [Eu(dpaC₁₂H₂₅)₃](NHET₃)₃ model compound.** A solution of EuCl₃·6H₂O (12 μL, 0.11 M, 1.4 μmol) in ethanol was added to a solution of dpaC₁₂H₂₅ (1.5 mg, 4.2 μmol), triethylamine (5.7 μL, 56 μmol) in CHCl₃ (3 mL). The reaction mixture was stirred at room temperature for 10 min and then directly used for analytical experiments. IR (cm⁻¹) 3097, 2922, 2852, 2499, 2048, 1694, 1648, 1596, 1570, 1455, 1423, 1378, 1310, 1278, 1117, 1038, 879, 803, 714, 635.

***In situ* preparation of model compound [Eu(MebipC₁₂H₂₅)₃](ClO₄)₃.** A solution of Eu(ClO₄)₃ (50 μL, 50% in H₂O) was diluted with CH₃CN (5.0 mL) and then dried over NaSO₄ and filtered. A portion of the anhydrous Eu(ClO₄)₃ solution (100 μL, 0.80 μmol) was added to a solution of MebipC₁₂H₂₅ (1.3 mg, 2.5 μmol) in CHCl₃ (2.5 mL). The solution was then stirred at room temperature for 30 min and directly used for analytical experiments. IR (cm⁻¹) 3446, 3060, 2920, 2850, 1589, 1565, 1477, 1467, 1456, 1442, 1425, 1412, 1386, 1361, 1327, 1309, 1290, 1242, 1183, 1154, 1081, 1029, 1005, 925, 899, 883, 875, 862, 795, 765, 747, 739, 699, 621.

3. Experimental procedures

Ultrasonication experiments. All ultrasonication experiments were performed with a Branson Model 450 ultrasonic 1/2 in horn sonicator with an attached 1/8 in tapered microtip. The length of the sonication pulses was varied as specified, and unless otherwise specified the amplitude was set to 20%. Ultrasonication experiments in solutions were conducted in cuvettes containing 3 mL of the respective solution with an initial temperature of 25 °C. Single sonication pulses caused a modest temperature increase, as detailed in Figure S19.

***In situ* monitoring of the ultrasound induced dissociation by photoluminescence spectroscopy.** A representative procedure is provided: An ultrasonicator was inserted into the top port of a PTI fluorimeter and the ultrasonicator microtip was placed into a Hellma 111-QS quartz cuvette which contained a polymer solution of [Eu(BKB)_{1.5}](ClO₄)₃ (2 mg/mL) in CHCl₃ (3 mL). The experimental setup was covered by a Thorlabs black rubberized fabric to eliminate any external illumination. The [Eu(BKB)_{1.5}](ClO₄)₃ solution was subjected to repeated ultrasonication pulses (5 × 10 sec) with a delay of 300 sec between each pulse. The [Eu(BKB)_{1.5}](ClO₄)₃ solution was excited at 378 nm and the emission of the ⁵D₀ → ⁷F₂ was monitored at 615 nm as a function of time.

Ultrasonication of Fe²⁺-imbibed polymer films. All experiments were performed at 0 °C with a pulse sequence of 0.5 sec and 1 sec delay for 60 min of total sonication time. A representative procedure is provided: A film of [Eu(BKB)_{1.5}](ClO₄)₃ (20 mg, ca. 200 μm thickness) was placed in a Fe(ClO₄)₂ solution (0.5 μM) in CH₃CN (10 mL) and swollen for 5 d until an equilibrium was reached. As specified for each experiment, either the Fe(ClO₄)₂ solution was subsequently cooled and the samples was ultrasonicated in this solution at 0 °C for 60 min or the sample was subsequently transferred into a cold CH₃CN (without any metal) and ultrasonicated for 60 min.

Welding of polymer films by ultrasonication. Dog-bone shaped films (150-250 μm thickness) were cut in half and the ends were then overlapped to create a lap-joint with an

overlap of ca. 2 mm. The samples were placed between two glass slides lined with Teflon® sheets. The films were then either submersed directly in CH₃CN or vacuum-sealed in a plastic bag and submersed in CH₃CN for ultrasonication. Ultrasonication was conducted at 0 °C for 1 h total pulse time (0.5 sec pulse, 1 sec delay time, 20% amplitude). All further characterizations were performed on the samples submersed directly.

Swelling behavior of polymer films. A representative procedure is provided. The swelling behavior of [Eu(BKB)_{1.5}](ClO₄)₃ (15 mg, 25 mm × 5 mm × 150 μm) thin films was investigated by immersing the samples in CH₃CN at room temperature for 10 d. The degree of swelling was determined by measuring the weight of the samples pre- and post-swelling:

$$\text{Degree of swelling (\%)} = \frac{\text{mass of wet sample} - \text{mass of dry sample}}{\text{mass of dry sample}} \times 100$$

To minimize the error in measuring the degree of swelling, samples were placed on filter paper to wick excess CH₃CN from the surface before they were weighed.

Small-angle X-Ray Scattering (SAXS). The SAXS spectra were recorded with an S-MAX3000 pinhole camera (Rigaku Innovative Technologies, Auburn Hills, USA). The samples were kept in vacuum at room temperature during the measurements. Raw data were processed according to standard procedures, and we present the scattering spectra as a function of the momentum transfer $q = 4\pi \cdot \lambda^{-1} \cdot \sin(\theta/2)$, where θ is the scattering angle and $\lambda = 0.1524$ nm is the photon wavelength.

Optical microscopy. The optical microscopy images were taken on an Olympus BX51 microscope equipped with a DP72 digital camera with a magnification of five times. The exposure times are given in the respective figure captions in the Supporting Information.

4. Supporting discussion

Supporting discussion of the Photophysical Experiments Conducted in Connection with the Ultrasound and Thermally Induced Dissociation of [Eu(BKB)_{1.5}](ClO₄)₃

The data shown in Figures S11, S12 and S19 and Figure 2 in the paper serve as basis for the discussion of the photophysical properties of [Eu(BKB)_{1.5}](ClO₄)₃ and changes caused by application of ultrasound and/or heat as external stimuli. The excitation and emission spectra of [Eu(BKB)_{1.5}](ClO₄)₃ in CHCl₃ (Figure 2a, Figure S12) reveal the existence of multiple excitation pathways. The observed luminescence associated with ⁵D₀ → ⁷F_J transitions ($\lambda_{\text{em}} = 615$ nm for the most prominent with $J = 2$) is a characteristic signature of europium complexes. The radiative excited state can be populated through *direct* excitation of the f-f transitions or by *indirect* excitation through the ligand and subsequent population of the D-states via a resonance energy transfer.⁵ An excitation scan of [Eu(BKB)_{1.5}](ClO₄)₃ in CHCl₃ in which the emission from the ⁵D₀ → ⁷F₂ transition ($\lambda_{\text{em}} = 615$ nm) is monitored, reveals a narrow excitation band with a λ_{max} of 375 nm (Figure 2a). This excitation spectrum does neither mirror the absorption spectrum of the metallopolymer nor that of the free BKB (Figure S11c). An excitation scan of [Eu(BKB)_{1.5}](ClO₄)₃ in CHCl₃ in which the emission from the ligand ($\lambda_{\text{em}} = 395$ nm) is monitored, reveals a broad excitation band ($\lambda_{\text{max}} = 332, 347$ nm, Figure S12b) which does resemble the absorption spectrum of the metallopolymer (Figure S11c). These findings are consistent with the well-established fact that europium complexes can often be more effectively excited via the ligand-to-metal-charge-transfer (LMCT) transition than via the ligand.⁵ As a consequence, absorption and excitation spectra do not match. Indeed, the formation of an LMCT band is evident in the absorption spectrum of [Eu(BKB)_{1.5}](ClO₄)₃ (Figure S11a, S11c).

Consistent with this interpretation, the emission spectra of [Eu(BKB)_{1.5}](ClO₄)₃ acquired upon excitation at $\lambda_{\text{exc}} = 375$ and 332 nm (Figure 2a and Figure S12b) show different relative contribution of ligand emission. The emission spectra obtained upon excitation at 375 nm (Figure 2a) show mainly the intense, sharp emission bands associated with europium complexes and only a minor contribution associated with ligand fluorescence ($\lambda_{\text{em}} = 400 - 550$ nm). By contrast, the emission spectra obtained upon excitation at 332 nm reveal a much more pronounced fluorescence of the ligand ($\lambda_{\text{em}} = 390 - 550$ nm) (Figure S12b), the absolute emission intensity is much lower (not shown, since data are normalized), and the signal-to-noise ratio of the europium emission is decreased.

Taken together, the data clearly show that the luminescence associated with the ⁵D₀ → ⁷F_J transition of [Eu(BKB)_{1.5}](ClO₄)₃ is most efficiently, and rather selectively, caused by excitation of the LMCT transition around 375 nm. Thus, the *in situ* monitoring of the ultrasound-induced dissociation of [Eu(BKB)_{1.5}](ClO₄)₃ is based on the fact that dissociation causes a reduction of the LMCT absorption at 375 nm. Since changes in absorbance are minor (cf. thermally induced dissociation experiments, Figure S19h), we opted to monitor this change via the reduction of the ⁵D₀ → ⁷F₂ emission ($\lambda_{\text{em}} = 615$ nm). At the same time, it is

⁵Richardson, F. S. *Chem. Rev.* **1982**, 82, 541.

feasible to monitor the dissociation through an increased emission of the free ligand; in this case, excitation must of course occur at 332-347 nm.

To explore the photophysical properties further, and to exclude dominant temperature effects, the (reversible) disassembly of $[\text{Eu}(\text{BKB})_{1.5}](\text{ClO}_4)_3$ in CHCl_3 was explored by temperature-dependent optical spectroscopy. Absorption spectra acquired at different concentrations (Figure S19g) and temperature (Figure S19h) show little variation, indicative of the fact that the equilibrium is in all cases far on the product ($[\text{Eu}(\text{BKB})_{1.5}](\text{ClO}_4)_3$) side. Photoluminescence experiments in which either the $^5\text{D}_0 \rightarrow ^7\text{F}_2$ emission ($\lambda_{\text{em}} = 615$ nm, Figure S19a, e) or the ligand emission ($\lambda_{\text{em}} = 469$ nm, Figure S19b,c) is monitored as a function of temperature, show a reversible decrease of the emission intensity as the temperature is increased, consistent with a reduction of the LMCT absorbance. The experiment was repeated, but the $[\text{Eu}(\text{BKB})_{1.5}](\text{ClO}_4)_3$ was excited via the ligand ($\lambda_{\text{exc}} = 332$ nm); in this case an increase in the ligand fluorescence ($\lambda_{\text{em}} = 395$ nm) and simultaneous a decrease in the emission of the $^5\text{D}_0 \rightarrow ^7\text{F}_2$ transition ($\lambda_{\text{em}} = 615$ nm) can be observed upon heating (Figure S19e). Also this experiment, which points to an increased concentration of free ligand and a decreased concentration of the emissive Eu^{3+} species, supports the postulated dissociation upon heating. The changes are fully reversible, i.e., the original properties are restored upon cooling.

Due to the photophysical properties of these materials and europium complexes, the equilibrium of the supramolecular polymerization of $[\text{Eu}(\text{BKB})_{1.5}](\text{ClO}_4)_3$ can be probed in multiple ways. The excitation of the LMCT allows for the observation of the europium complex while minimizing the contributions of the decay pathways of the ligand. Excitation via the ligand allows monitoring both the contributions of the ligand and europium complex. Since equilibria of supramolecular polymerizations are complex,⁶ especially if based on metal-ligand complexes,⁵ the excitation through the LMCT allows for the observation of Eu^{3+} complex while minimizing contributions from various other species and decay pathways.

Since temperature changes can also cause depolymerization of $[\text{Eu}(\text{BKB})_{1.5}](\text{ClO}_4)_3$ and thereby cause spectroscopic changes that could be mis-interpreted as being the result of mechanically induced dissociation, comparative experiments were conducted to separate these effects. In Figure 2f the emission of the $^5\text{D}_0 \rightarrow ^7\text{F}_2$ transition ($\lambda_{\text{em}} = 615$ nm) of $[\text{Eu}(\text{BKB})_{1.5}](\text{ClO}_4)_3$ in CHCl_3 was plotted as a function of temperature for samples that were either deliberately heated or exposed to ultrasonication pulses of various durations; in case of the latter, the temperature increase induced by sonication was measured and the data are plotted accordingly. The figure shows clearly that the mechanochemical effect induced by ultrasonication clearly outweighs the effect caused by sonication-induced heating. For instance, a 10 s ultrasonication pulse results in a ca. 17 % decrease in emission intensity at 615 nm, whereas less than a 1.5% decrease in emission is observed at 31 °C, the temperature of CHCl_3 after a 10 s ultrasonication pulse (Figure 2f). Gratifyingly, the relaxation kinetics of samples dissociated thermally and by exposure to ultrasonication are virtually identical (Figure S19e), suggesting that the species involved are the same.

⁶Brunsveld, L.; Folmer, B. J. B.; Meijer, E. W.; Sijbesma, R. P. *Chem. Rev.* **2001**, *101*, 4071.

5. Supporting figures

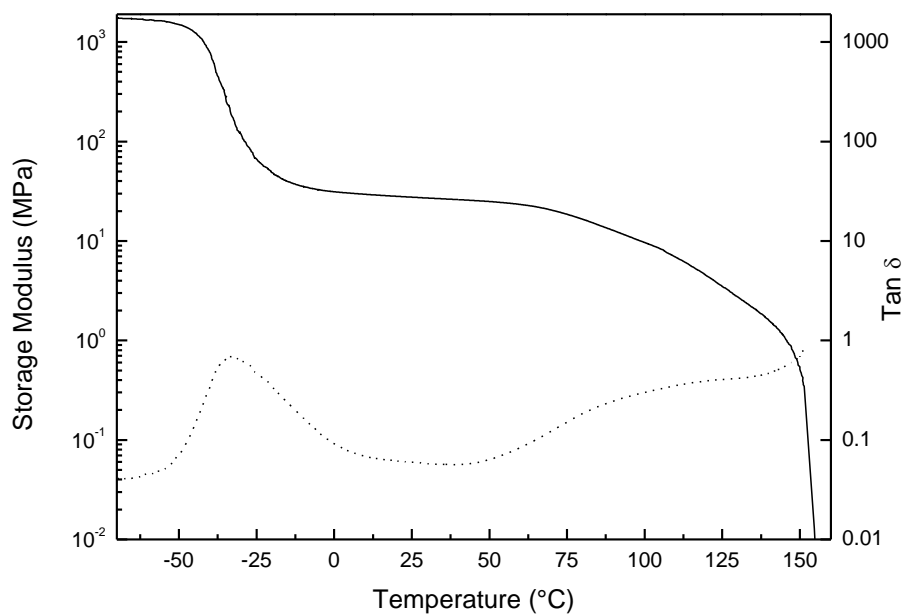


Figure S1. Mechanical analysis of [Eu(BKB)_{1.5}](ClO₄)₃. Representative dynamic mechanical thermal analysis (DMTA) traces of [Eu(BKB)_{1.5}](ClO₄)₃ (ca. 200 μm thickness) from -70 to 160 °C; storage modulus (—) and tan δ (⋯). Experiments were conducted under N₂ atmosphere at a heating rate of 3 °C/min and a frequency of 1 Hz. At 25 °C, the storage modulus is 23 ± 6 MPa.

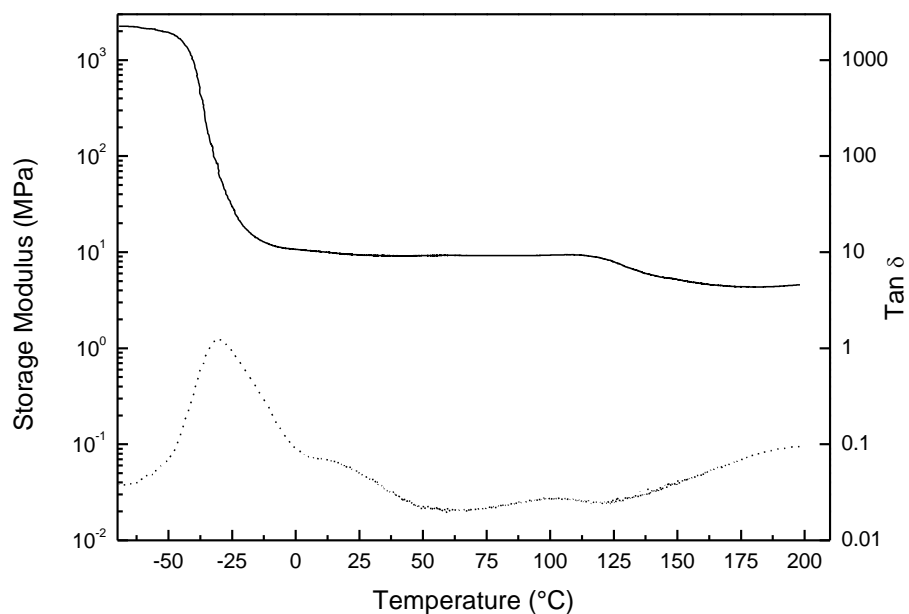


Figure S2. Mechanical analysis of $[\text{Eu}(\text{DKD})_{1.5}](\text{NH}_4\text{Et}_3)_3$. Representative dynamic mechanical thermal analysis (DMTA) traces of $[\text{Eu}(\text{DKD})_{1.5}](\text{NH}_4\text{Et}_3)_3$ (ca. 200 μm thickness) from -70 to 200 $^\circ\text{C}$; storage modulus (—) and $\tan \delta$ (⋯). Experiments were conducted under N_2 atmosphere at a heating rate of 3 $^\circ\text{C}/\text{min}$ and a frequency of 1 Hz. At 25 $^\circ\text{C}$, the storage modulus is 8 ± 1.5 MPa.

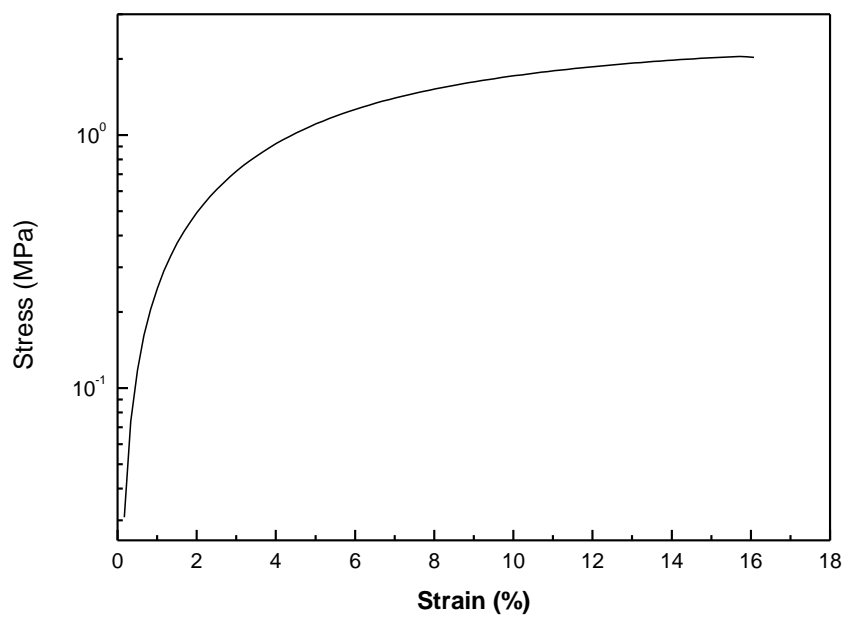


Figure S3. Mechanical analysis of $[\text{Eu}(\text{BKB})_{1.5}](\text{ClO}_4)_3$. Representative stress-strain curve of $[\text{Eu}(\text{BKB})_{1.5}](\text{ClO}_4)_3$. Measurements were conducted under N_2 atmosphere at 25 °C, with a strain rate of 5%/min.

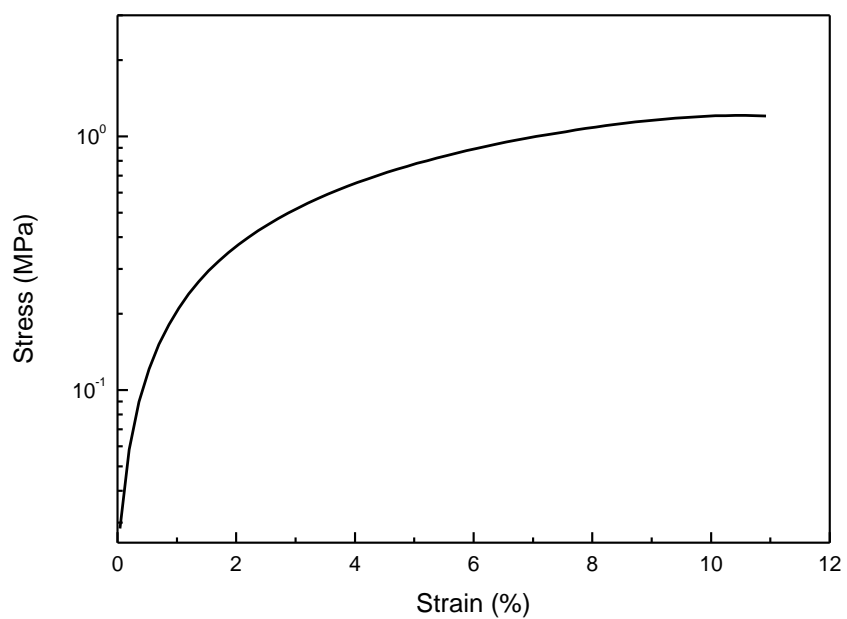


Figure S4. Mechanical analysis of $[\text{Eu}(\text{DKD})_{1.5}](\text{NH}_4\text{Et}_3)_3$. Representative stress-strain curve of $[\text{Eu}(\text{DKD})_{1.5}](\text{NH}_4\text{Et}_3)_3$. Measurements were conducted under N_2 atmosphere at $25\text{ }^\circ\text{C}$, with a strain rate of $5\%/ \text{min}$.

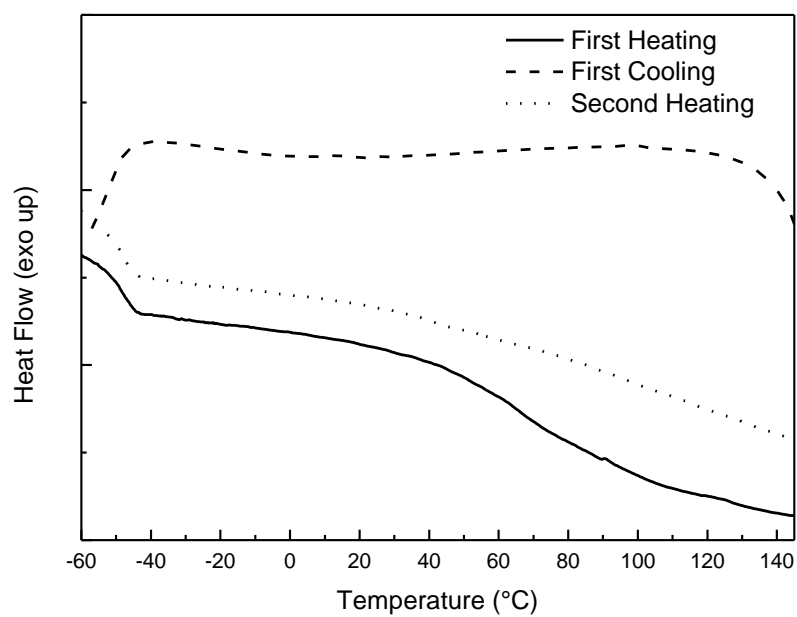


Figure S5. Thermal analysis of [Eu(BKB)_{1.5}](ClO₄)₃. Modulated differential scanning calorimetry (DSC) curves of [Eu(BKB)_{1.5}](ClO₄)₃; first heating (—), first cooling (- - -) and second heating (···). The experiment was conducted with heating and cooling rates of 10° C/min under N₂ atmosphere.

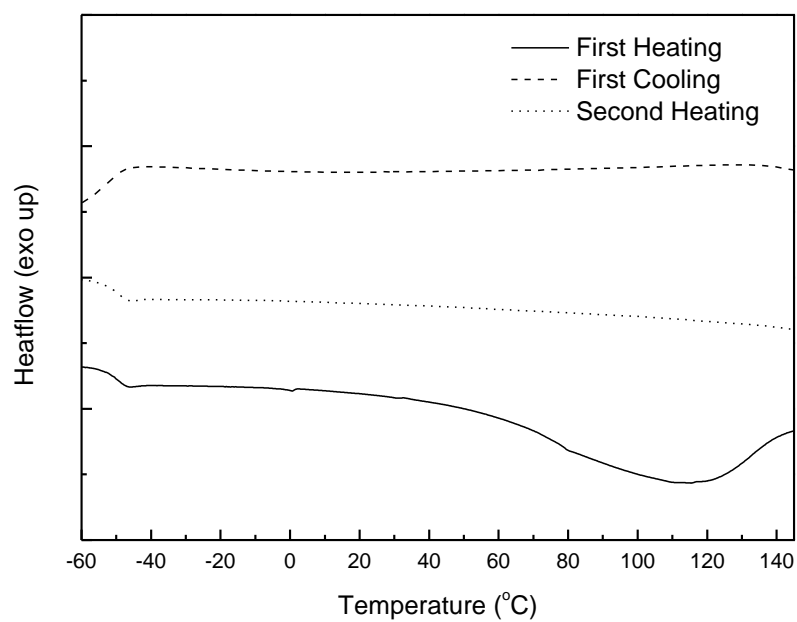


Figure S6. Thermal analysis of [Eu(DKD)_{1.5}](NHEt₃)₃. Modulated differential scanning calorimetry (DSC) curves of [Eu(DKD)_{1.5}](NHEt₃)₃; first heating (—), first cooling (- - -) and second heating (···). The experiment was conducted with heating and cooling rates of 10° C/min under N₂ atmosphere.

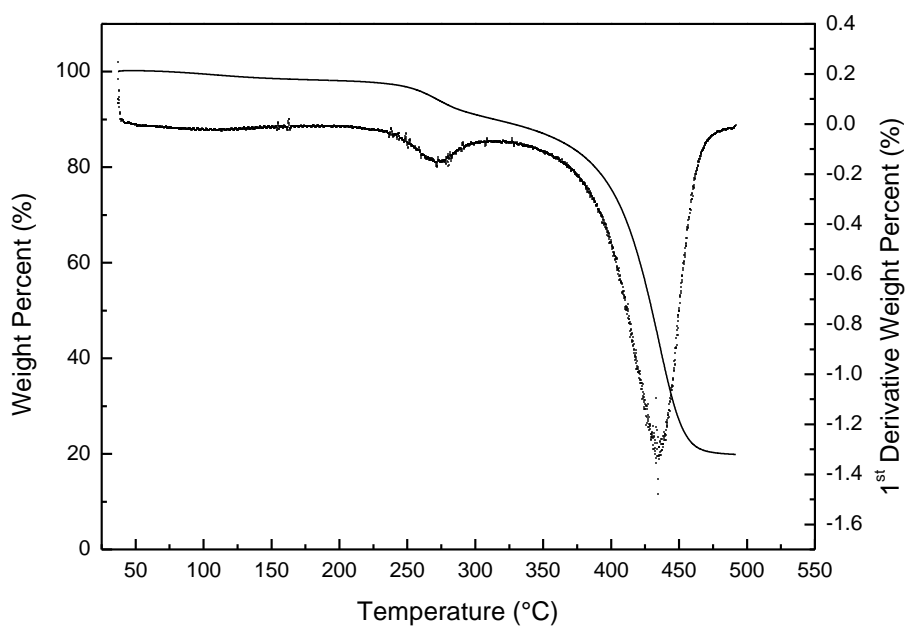


Figure S7. Thermal analysis of $[\text{Eu}(\text{BKB})_{1.5}](\text{ClO}_4)_3$. Thermogravimetric analysis (TGA) curves of $[\text{Eu}(\text{BKB})_{1.5}](\text{ClO}_4)_3$ from 25 to 500 °C; weight percent (—) and derivative weight percent (···). The experiment was conducted at a heating rate of 10° C/min under N_2 atmosphere.

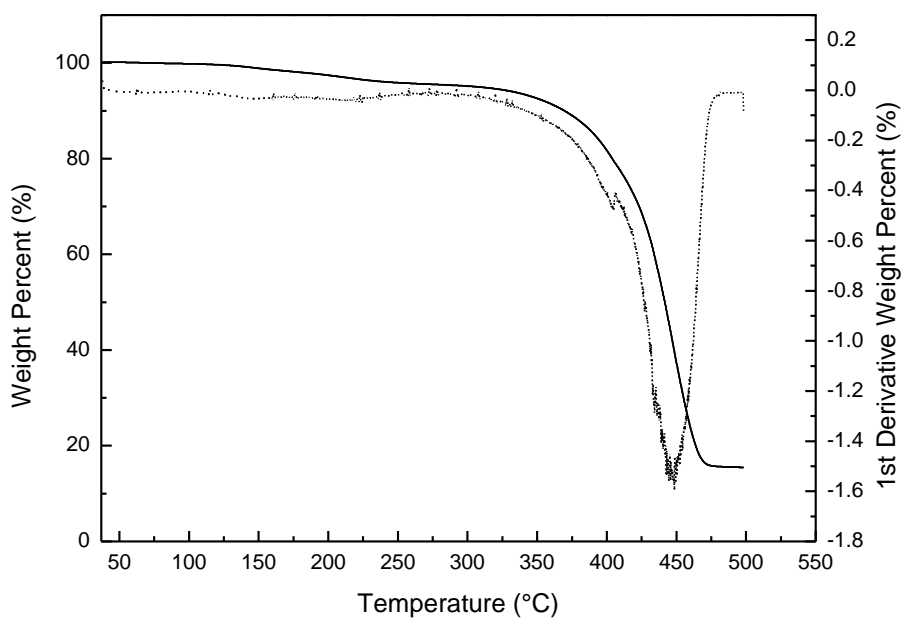


Figure S8. Thermal analysis of [Eu(DKD)_{1.5}](NH₄Et₃)₃. Thermogravimetric analysis (TGA) curves of [Eu(DKD)_{1.5}](NH₄Et₃)₃ from 25 to 500 °C; weight percent (—) and derivative weight percent (···). The experiment was conducted at a heating rate of 10° C/min under N₂ atmosphere.

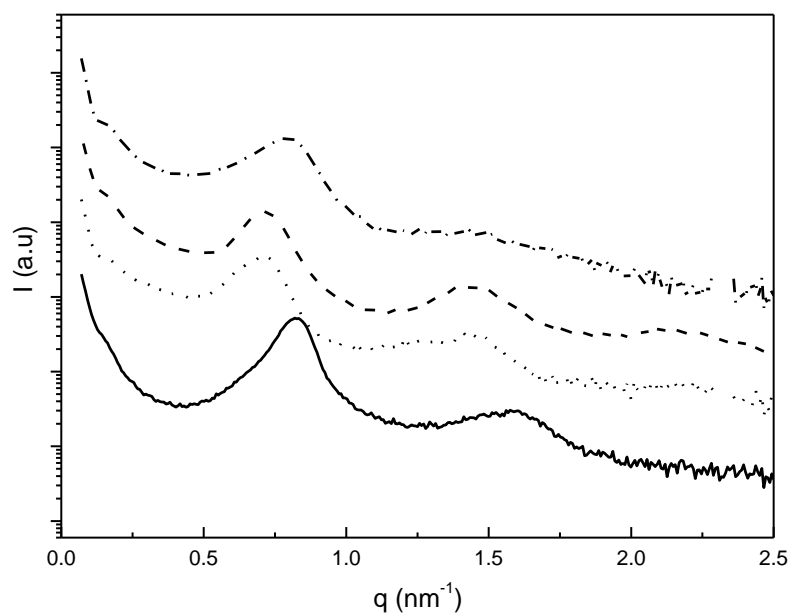


Figure S9. Morphology characterization of $[\text{Eu}(\text{BKB})_{1.5}](\text{ClO}_4)_3$. Small-angle X-ray scattering (SAXS) data for $[\text{Eu}(\text{BKB})_{1.5}](\text{ClO}_4)_3$ under various conditions; the curves are shifted vertically for clarity. As-prepared film (—) with a lamellar period of 7.3 nm; film after swelling in CH_3CN for 24 h and drying in vacuum for 12 h (- - -) with a lamellar period of 8.7 nm; film after swelling in $\text{Fe}(\text{ClO}_4)_2$ solution (0.5 mM, CH_3CN , 5 days) and ultrasonication for 1 h while immersed in the $\text{Fe}(\text{ClO}_4)_2$ solution with 8.8 nm as lamellar period (\cdots). The SAXS data of a $[\text{Fe}(\text{BKB})_{1.0}](\text{ClO}_4)_2$ reference film are also shown (— · —) with a lamellar period of 7.6 nm. This sample was made by combining one molar equivalent of BKB with 1 molar equivalent of $\text{Fe}(\text{ClO}_4)_2$ in a mixture of CHCl_3 and acetonitrile, evaporation of the solvents and subsequent compression-molding, under conditions that mirrored the process for the preparation of $[\text{Eu}(\text{BKB})_{1.5}](\text{ClO}_4)_3$.

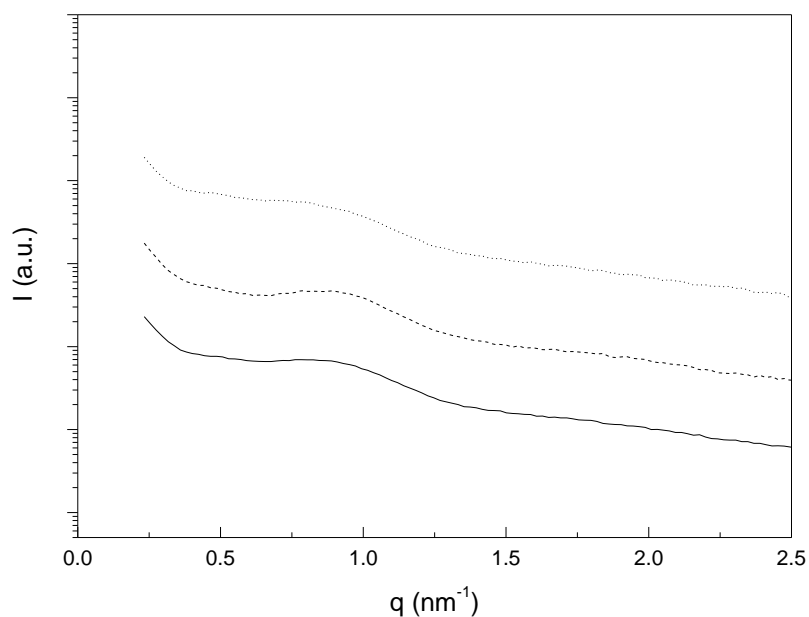


Figure S10. Morphology characterization of $[\text{Eu}(\text{DKD})_{1.5}](\text{NH}_4\text{Et}_3)_3$. Small-angle X-ray scattering (SAXS) data for $[\text{Eu}(\text{DKD})_{1.5}](\text{NH}_4\text{Et}_3)_3$ under various conditions; the curves are shifted vertically for clarity. As-prepared film (—); film after swelling in $\text{Fe}(\text{ClO}_4)_2$ solution (0.5 mM in CH_3CN , 5 days) and drying in vacuum for 12 h (- - -); film after swelling in $\text{Fe}(\text{ClO}_4)_2$ solution (0.5 mM in CH_3CN , 5 days) and ultrasonication for 1 h (⋯).

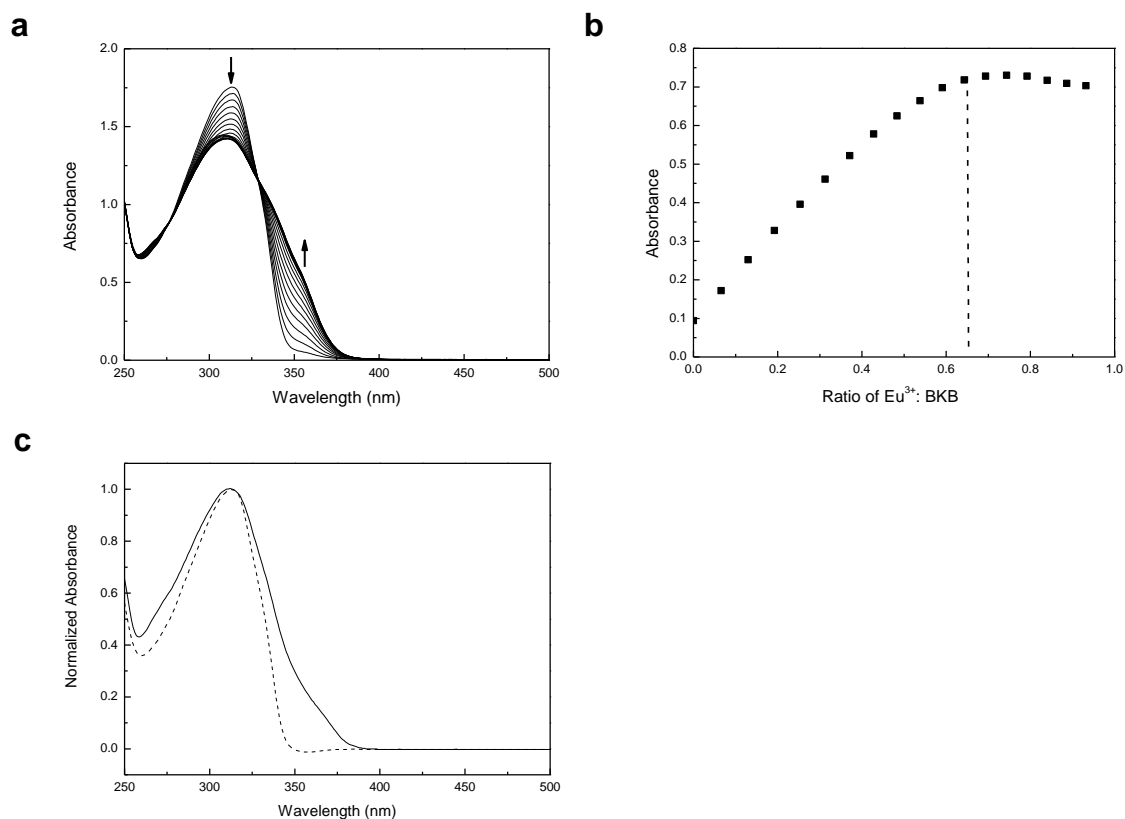


Figure S11. Titration of BKB with $\text{Eu}(\text{ClO}_4)_2$. **a**, UV-vis absorption spectra acquired upon titration of BKB ($25 \mu\text{M}$) in 9:1 CHCl_3 : CH_3CN (v/v) with aliquots of $\text{Eu}(\text{ClO}_4)_3$. Shown are absorption spectra with Eu^{3+} :BKB ratios ranging between 0 and 1.0. **b**, Plot of the absorbance at 347 nm as a function of the Eu^{3+} :BKB ratio. The appearing shoulder corresponds to the formation of the $[\text{Eu}(\text{BKB})_{1.5}](\text{ClO}_4)_3$ metal-ligand complex and the dashed line indicates the end point of the titration corresponding to a Eu^{3+} : BKB ratio of 0.66:1. **c**, Overlay of UV-vis absorption spectra of $[\text{Eu}(\text{BKB})_{1.5}](\text{ClO}_4)_3$ (—) and BKB(---) in CHCl_3 solution (0.5 mg/mL).

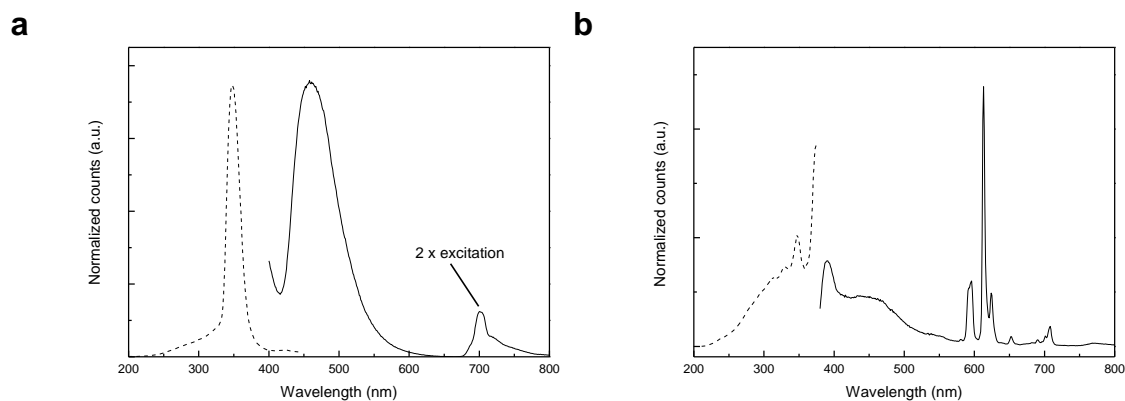


Figure S12. Emission spectra of neat BKB and metallopolymer $[\text{Eu}(\text{BKB})_{1.5}](\text{ClO}_4)_3$ in CHCl_3 . **a**, Excitation (---) and emission (—) spectra of neat BKB in CHCl_3 (2 mg/mL). Excitation and emission spectra were recorded with detection at 460 nm (emission maximum of the free Mebip ligand) and excitation at 347 nm (absorption maximum of the free Mebip ligand), respectively. **b**, Excitation (---) and emission (—) spectra of $[\text{Eu}(\text{BKB})_{1.5}](\text{ClO}_4)_3$ in CHCl_3 (2 mg/mL). Excitation and emission spectra were recorded with detection at 395 nm (maximum emission of the Eu^{3+} -bound Mebip ligand) and excitation at 332 nm (absorption of the Eu^{3+} -bound Mebip ligand), respectively.

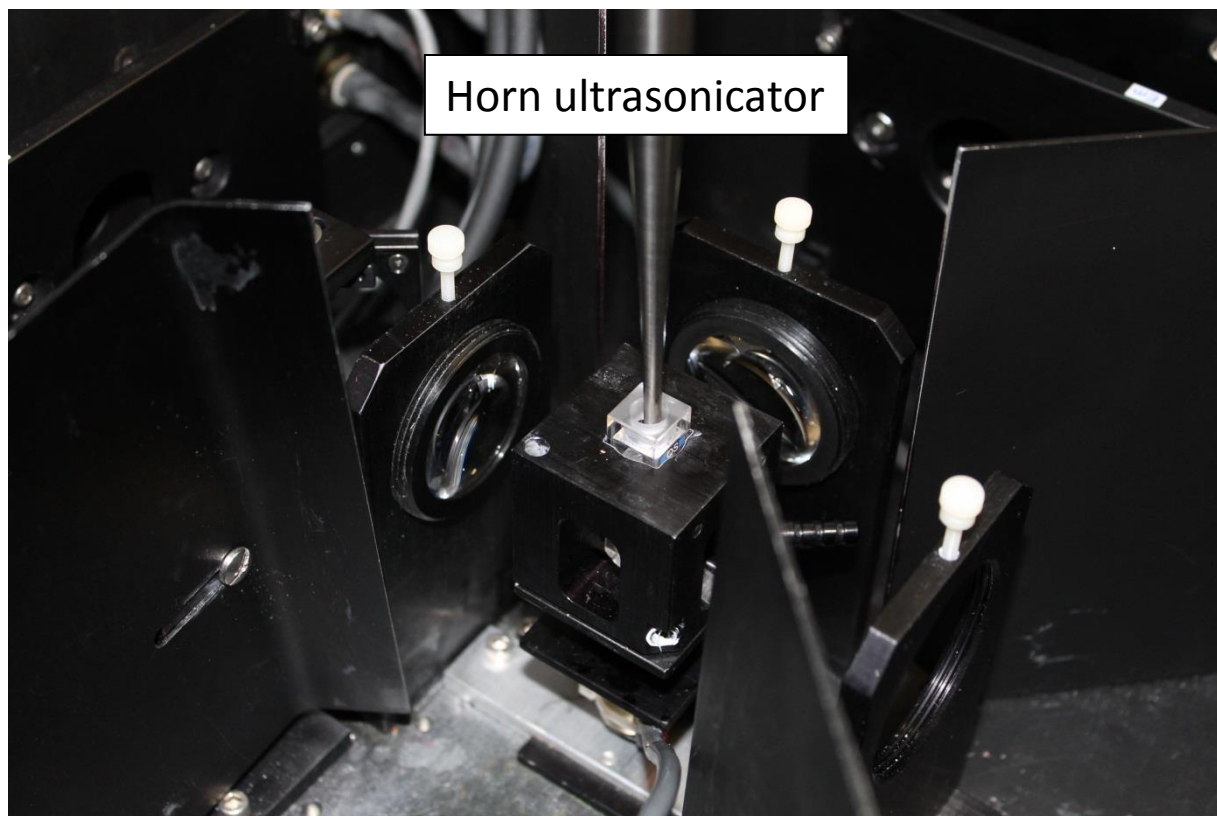


Figure S13. Image of experimental setup for photoluminescence studies. A horn ultrasonicator was positioned through the top port of a fluorimeter for *in situ* monitoring of the photoluminescence during ultrasonication.

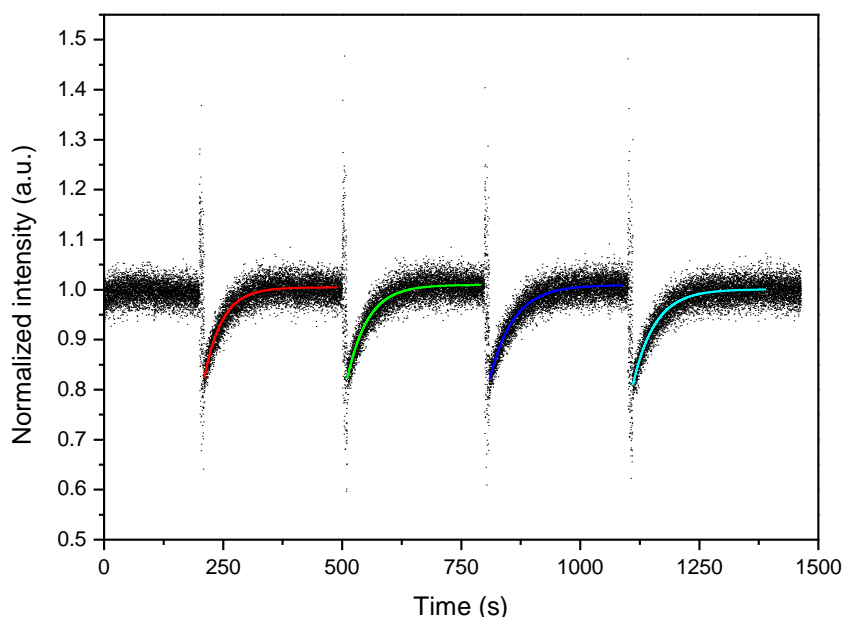


Figure S14. *In situ* monitoring of the ultrasound induced dissociation of $[\text{Eu}(\text{BKB})_{1.5}](\text{ClO}_4)_3$ and modeling of the photoluminescence recovery. Normalized emission intensity of the Eu^{3+} : ${}^5\text{D}_0 \rightarrow {}^7\text{F}_2$ transition ($\lambda = 615 \text{ nm}$) in a solution of $[\text{Eu}(\text{BKB})_{1.5}](\text{ClO}_4)_3$ in CHCl_3 (2.0 mg/ml). The solution was subjected to four ultrasonication pulses (10 sec each). The recovery was fitted to the single exponential equation $f(t) = 1 - e^{-(a+b \times (t - t_0))}$ described below. For the different pulses, values for a were found to be 1.71, 1.69, 1.68 and 1.65 and b 0.026, 0.023, 0.020 and 0.022, respectively.

To model the time dependence of photoluminescence recovery, we used the following assumptions:

- 1) Absorption (A) is dominant and scattering is negligible
 - Then: $A + T = 1, A = 1 - T$ (T= transmission)
- 2) Events of absorption are uncorrelated
 - Beer-Lambert law is justified: $T = e^{-\alpha N}$, where α is the absorption coefficient and N is the overall number of luminescent centers
- 3) Intensity of photoluminescence is linearly proportional to absorption
 - $I = i \times (1 - e^{-\alpha N})$
- 4) Recovery of luminescent centers is a linear function of time
 - $N(t > t_0) = N_0 + \beta t$, where β is the rate of recovery, t_0 is the time where sonication stops, and $N_0 = N(t = t_0)$.

With these assumptions the photoluminescence recovery is a following function of time: $f(t) = 1 - e^{-(a+b \times (t - t_0))}$ where $a = \alpha N_0$ and $b = \alpha \beta$.

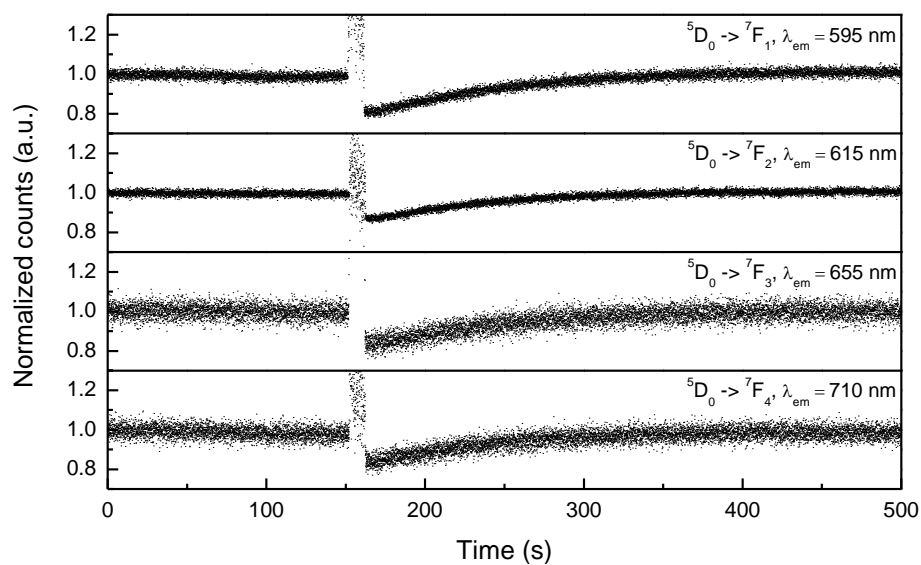


Figure S15. *In situ* monitoring of the ultrasound induced dissociation of $[\text{Eu}(\text{BKB})_{1.5}](\text{ClO}_4)_3$ by photoluminescence spectroscopy. Solutions of $[\text{Eu}(\text{BKB})_{1.5}](\text{ClO}_4)_3$ in CHCl_3 (2.0 mg/ml) were subjected to one sonication pulse with a duration of 10 sec. The samples were excited at 375 nm and the intensity of the various $\text{Eu}^{3+} {}^5\text{D}_0 \rightarrow {}^7\text{F}_J$ emission bands was monitored at the corresponding wavelengths ($\lambda_{\text{em}} = 595, 615, 655, 710$ nm) as a function of time.

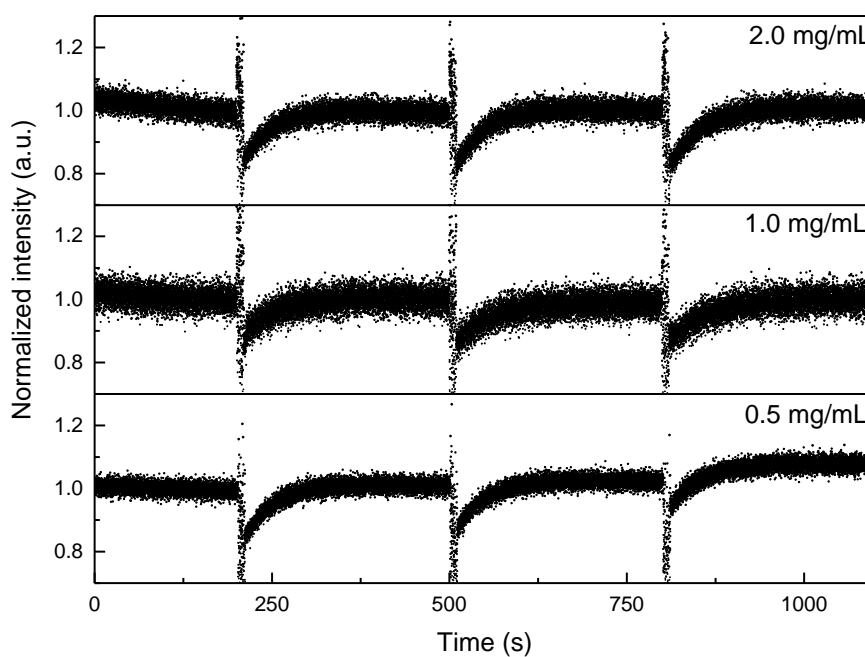


Figure S16. *In situ* monitoring of the ultrasound induced dissociation of [Eu(BKB)_{1.5}](ClO₄)₃ by photoluminescence spectroscopy. Solutions of [Eu(BKB)_{1.5}](ClO₄)₃ in CHCl₃ (2.0, 1, or 0.5 mg/ml) were subjected to three sonication pulses with a duration of 10 sec each. The samples were excited at 375 nm and the intensity of the Eu³⁺ ⁵D₀ → ⁷F₂ emission band was monitored at 615 nm as a function of time.

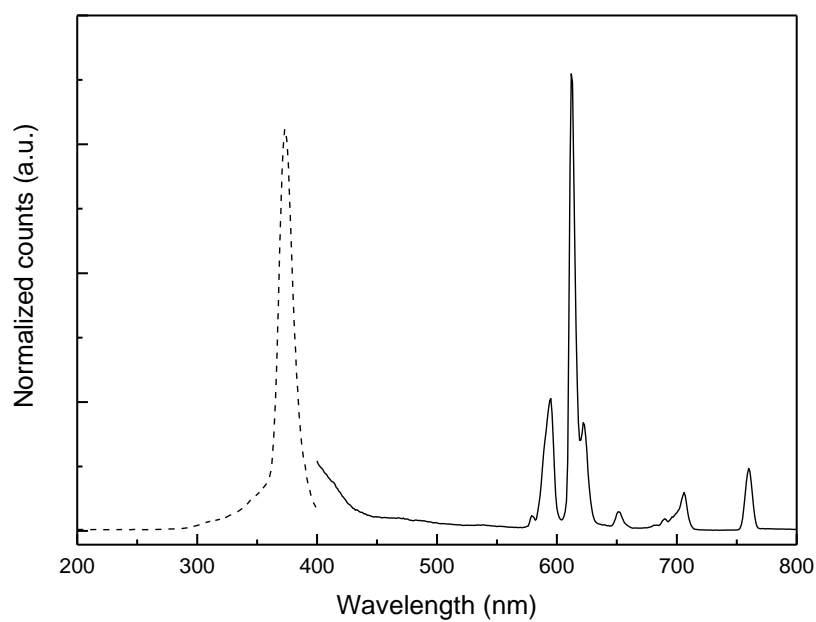


Figure S17. Excitation and emission spectra of model compound [Eu(MebipC₁₂H₂₅)₃](ClO₄)₃ in CHCl₃. Excitation (- - -) and emission (—) spectra of [Eu(MebipC₁₂H₂₅)₃](ClO₄)₃ in CHCl₃ (0.30 mM). Excitation and emission spectra were recorded with detection at 615 nm and excitation at 375 nm, respectively.

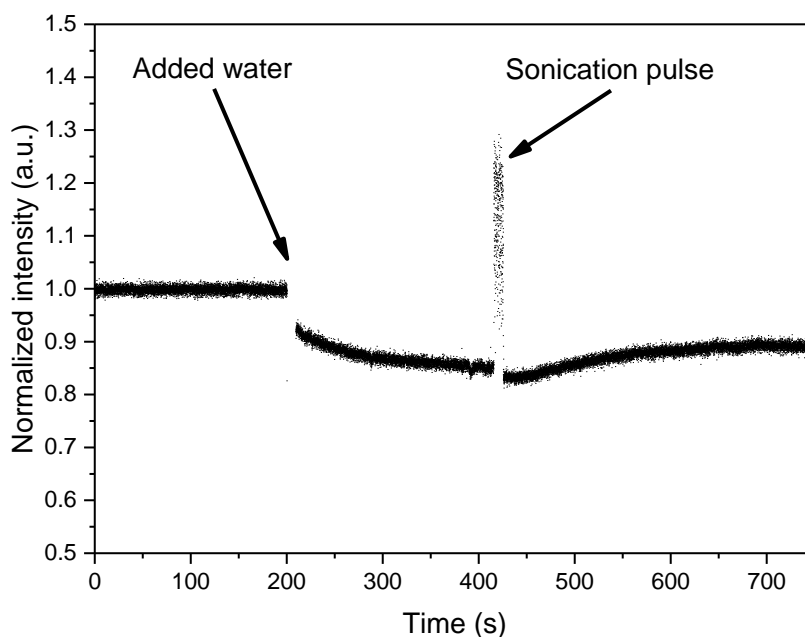


Figure S18. *In situ* monitoring of the ultrasound induced dissociation of $[\text{Eu}(\text{MebipC}_{12}\text{H}_{25})_3](\text{ClO}_4)_3$ after the addition of 26 equivalents of water by photoluminescence spectroscopy. A solution of $[\text{Eu}(\text{MebipC}_{12}\text{H}_{25})_3](\text{ClO}_4)_3$ in CHCl_3 (0.3 mM) was subjected to a sonication pulse with a duration of 10 sec after the addition of water. The samples were excited at 375 nm and the intensity of the $\text{Eu}^{3+5}\text{D}_0 \rightarrow {}^7\text{F}_2$ emission band was monitored at 615 nm as a function of time.

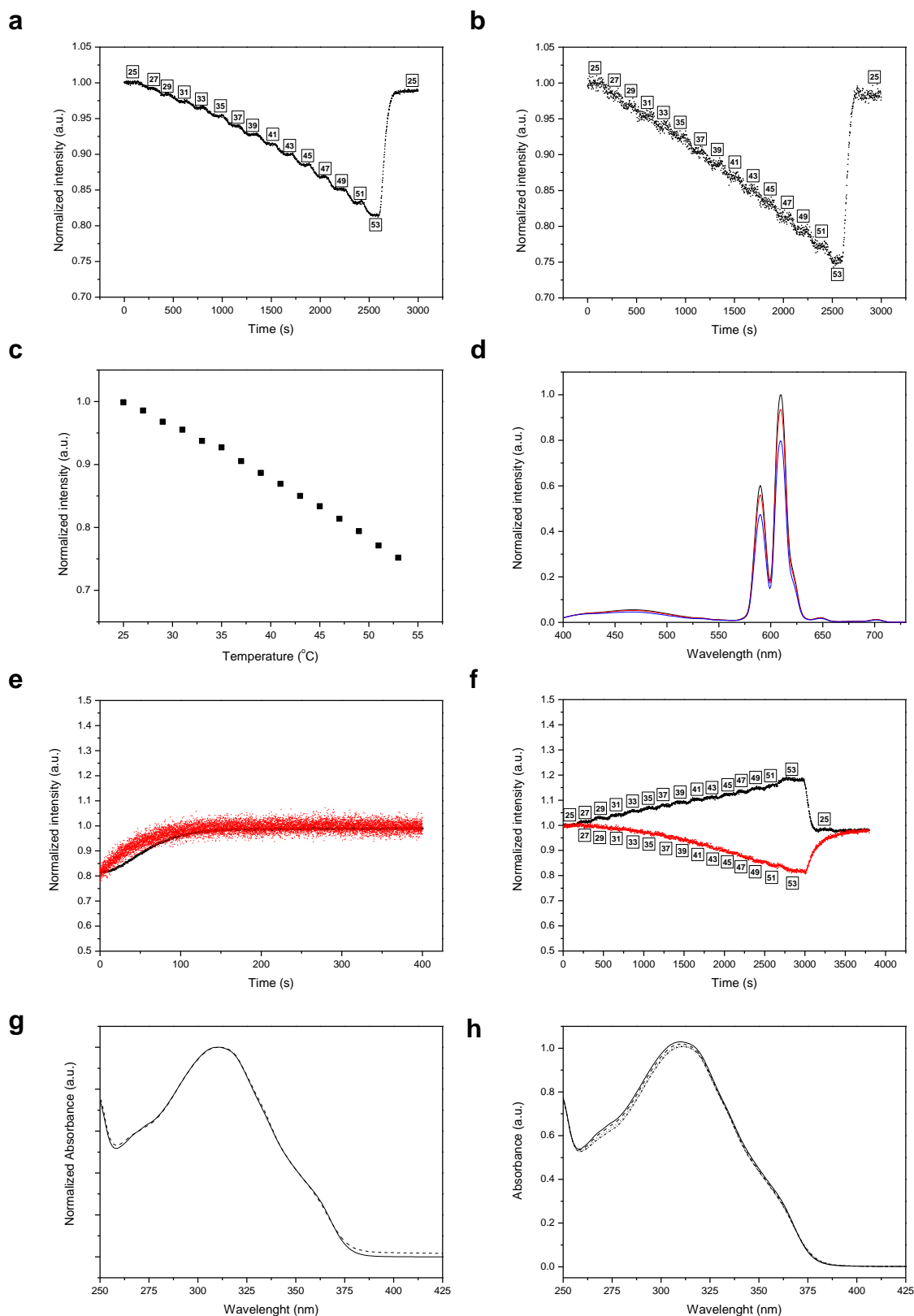


Figure S19. Comparison of the temperature-induced and ultrasonication-induced dissociation of $[\text{Eu}(\text{BKB})_{1.5}](\text{ClO}_4)_3$ monitored by photoluminescence spectroscopy. **a**, Normalized emission intensity of the $\text{Eu}^{3+} \text{D}_0 \rightarrow {}^7\text{F}_2$ transition (monitored at $\lambda_{\text{em}} = 615 \text{ nm}$) of $[\text{Eu}(\text{BKB})_{1.5}](\text{ClO}_4)_3$ in CHCl_3 (2.0 mg/ml) at different temperatures. The sample was excited

at 375 nm and the emission was monitored as a function of time, while increasing the temperature in discrete steps, as indicated in the graph. **b**, Normalized emission intensity of the Mebip fluorescence (monitored at $\lambda_{em} = 469$ nm) of $[\text{Eu}(\text{BKB})_{1.5}](\text{ClO}_4)_3$ in CHCl_3 (2.0 mg/ml) at different temperatures. The sample was excited at 375 nm and the emission was monitored as a function of time, while increasing the temperature in discrete steps, as indicated in the graph. **c**, Normalized emission intensity of the Mebip fluorescence (monitored at $\lambda_{em} = 469$ nm) of $[\text{Eu}(\text{BKB})_{1.5}](\text{ClO}_4)_3$ in CHCl_3 (2.0 mg/ml) at different temperatures. The values were extracted from the graph shown in part **b** permitting for 1 min of equilibration after each temperature increase. **d**, Emission spectra of $[\text{Eu}(\text{BKB})_{1.5}](\text{ClO}_4)_3$ in CHCl_3 (2 mg/mL) at 25 °C (—), 37 °C (—), and 53 °C (—). The sample was excited at 375 nm. **e**, Overlay of luminescence recovery experiments of $[\text{Eu}(\text{BKB})_{1.5}](\text{ClO}_4)_3$ in CHCl_3 (2.0 mg/ml) (monitored at $\lambda_{em} = 615$ nm, excited at 375 nm). The solutions had been subjected to either a 10 sec ultrasonication pulse (⋯, data were extracted from **Figure 2c** in the paper) or heated to 53 °C and rapidly cooled to 25 °C (—, data were extracted from the graph shown in part **a**). **f**, Normalized emission intensity of the Mebip fluorescence (monitored at $\lambda_{em} = 395$ nm, black dots) and the $\text{Eu}^{3+5}\text{D}_0 \rightarrow {}^7\text{F}_2$ transition (monitored at $\lambda_{em} = 615$ nm, red dots) of $[\text{Eu}(\text{BKB})_{1.5}](\text{ClO}_4)_3$ in CHCl_3 (2.0 mg/ml) at different temperatures. The sample was excited at 332 nm, where the ligand absorption is maximal, and not at 375 nm, where the absorption is caused by the LMCT, as in parts **a** or **b**), and the emission was monitored over time. **g**, Normalized absorption spectra of $[\text{Eu}(\text{BKB})_{1.5}](\text{ClO}_4)_3$ in CHCl_3 at concentrations of 1 mg/ml (—) and 0.1 mg/ml (- - -). **h**, Absorption spectra of $[\text{Eu}(\text{BKB})_{1.5}](\text{ClO}_4)_3$ in CHCl_3 at 25 °C (—), 35 °C (- - -), 45 °C (⋯), 53 °C (- ⋯ -). Data shown in parts **a** – **f** were recorded on a Jasco V-630 Spectrophotometer equipped with a Jasco ETC-272T Temperature Controller. The spectra shown in parts **g** and **h** were recorded on a Jasco V-670 Spectrophotometer equipped with a Jasco ETCR-762 Temperature Controller.

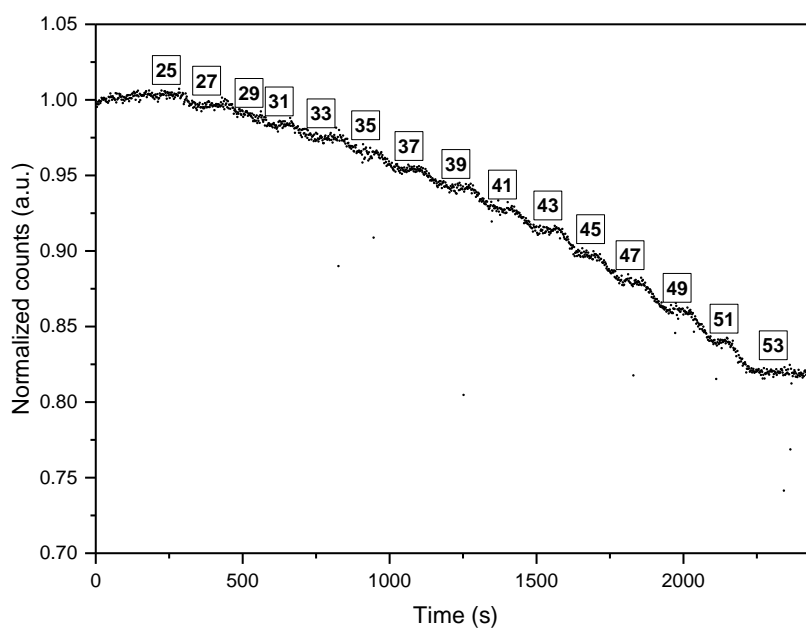


Figure S20. *In situ* monitoring of the temperature-induced dissociation of model compound $[\text{Eu}(\text{MebipC}_{12}\text{H}_{25})_3](\text{ClO}_4)_3$ in CHCl_3 . Normalized emission intensity of the $\text{Eu}^{3+}{}^3\text{D}_0 \rightarrow {}^7\text{F}_2$ transition (monitored at $\lambda_{\text{em}} = 615 \text{ nm}$) of $[\text{Eu}(\text{MebipC}_{12}\text{H}_{25})_3](\text{ClO}_4)_3$ in CHCl_3 (2.0 mg/ml) at different temperatures. The sample was excited at 375 nm and the emission was monitored as a function of time, while increasing the temperature in discrete steps, as indicated in the graph.

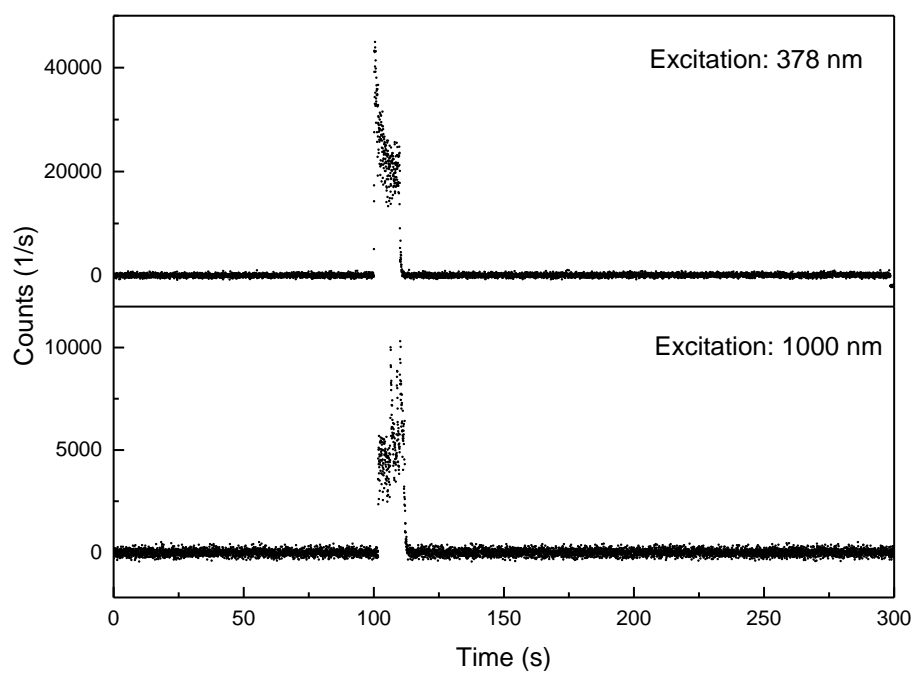


Figure S21. Sonoluminescence of CHCl_3 . CHCl_3 was subjected to one ultrasonication pulse with a duration of 10 sec. The solution was excited at various wavelengths (top: $\lambda_{\text{ex}} = 375$ nm; bottom: $\lambda_{\text{ex}} = 1000$ nm) and the emission was monitored at 615 nm. The response was found to be independent of the excitation wavelength.

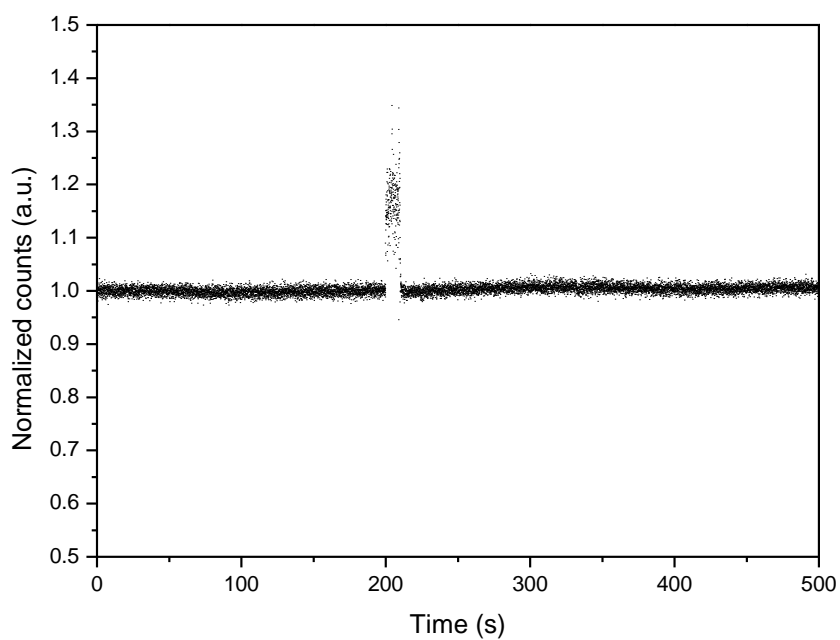


Figure S22. *In situ* monitoring of ultrasound induced changes of the neat BKB monomer by photoluminescence spectroscopy. A solution of BKB in CHCl_3 (2.0 mg/ml) was subjected to one sonication pulse with a duration of 10 sec. The solution was excited at 347 nm and the emission was monitored at 440 nm.

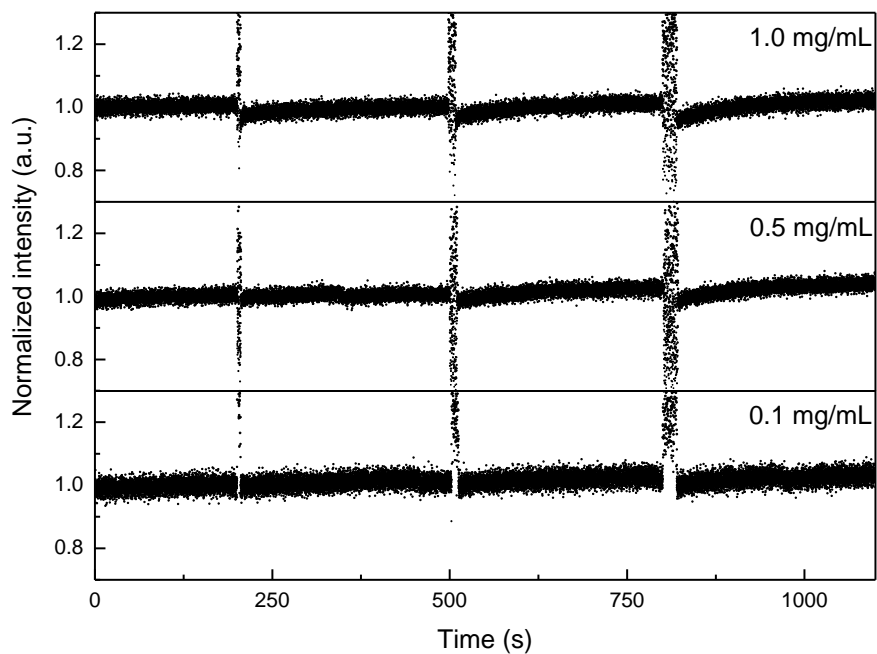


Figure S23. *In situ* monitoring of the ultrasound induced dissociation of $[\text{Eu}(\text{DKD})_{1.5}](\text{NHEt}_3)_3$. Solutions of $[\text{Eu}(\text{DKD})_{1.5}](\text{NHEt}_3)_3$ in CHCl_3 (1.0, 0.5, 0.1 mg/ml) were subjected to three sonication pulses with a duration of 5, 10, and 20 sec. The samples were excited at 275 nm and the intensity of the $\text{Eu}^{3+} {}^5\text{D}_0 \rightarrow {}^7\text{F}_2$ emission band was monitored at 615 nm.

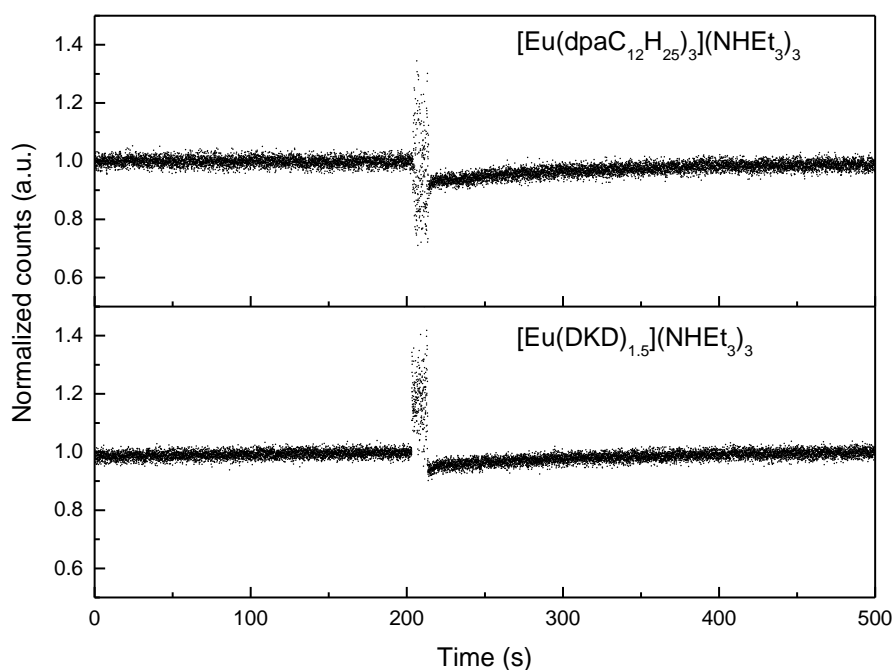


Figure S24. *In situ* monitoring of the ultrasound induced dissociation of model compound $[\text{Eu}(\text{dpaC}_{12}\text{H}_{25})_3](\text{NH}_4\text{Et}_3)_3$ and of $[\text{Eu}(\text{DKD})_{1.5}](\text{NH}_4\text{Et}_3)_3$ by photoluminescence spectroscopy. Top: A solution of $[\text{Eu}(\text{dpaC}_{12}\text{H}_{25})_3](\text{NH}_4\text{Et}_3)_3$ in CHCl_3 (0.47 mM) was subjected to one sonication pulse with a duration of 10 sec (20% amplitude). The solution was excited at 275 nm and the emission was monitored at 615 nm. Bottom: A solution of $[\text{Eu}(\text{DKD})_{1.5}](\text{NH}_4\text{Et}_3)_3$ in CHCl_3 (1 mg/ml, $[\text{Eu}^{3+}] = 0.33$ mM) was subjected to one sonication pulse with a duration of 10 sec. The solution was excited at 275 nm and the emission was monitored at 615 nm.

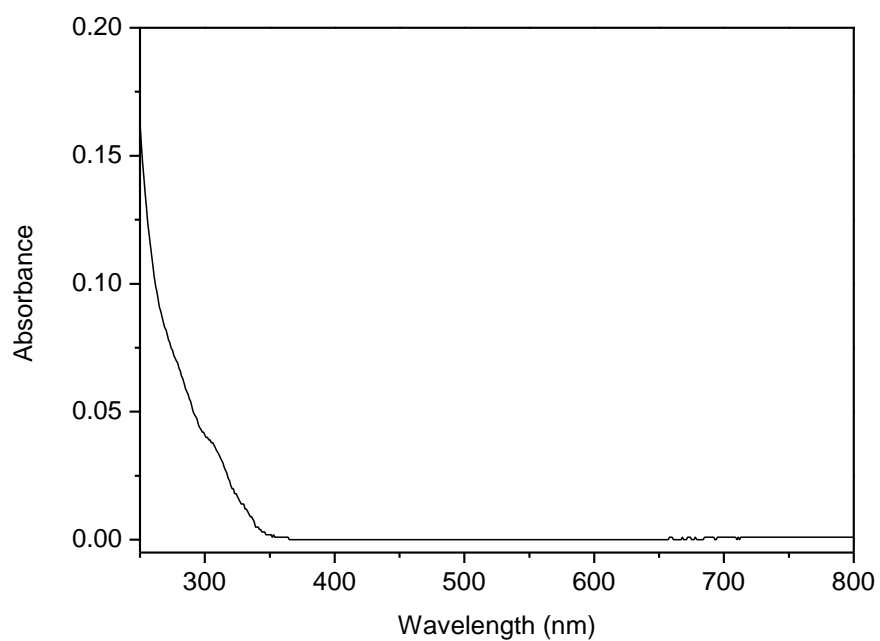


Figure S25. UV-Vis absorption spectrum of $[\text{Eu}(\text{DKD})_{1.5}](\text{NH}_4\text{Et}_3)_3$ in CHCl_3 (0.1 mg/mL).

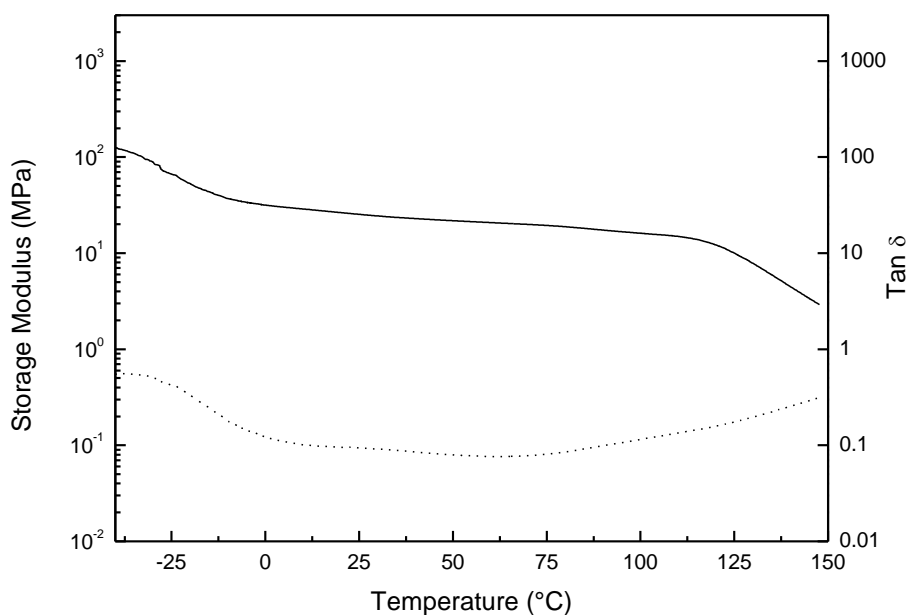


Figure S26. Mechanical analysis of welded films of $[\text{Eu}(\text{BKB})_{1.5}](\text{ClO}_4)_3$. Representative dynamic mechanical thermal analysis (DMTA) trace of an ultrasound-welded film of $[\text{Eu}(\text{BKB})_{1.5}](\text{ClO}_4)_3$ from -30 to 150 °C; storage modulus (—) and $\tan \delta$ (···). Cut films of $[\text{Eu}(\text{BKB})_{1.5}](\text{ClO}_4)_3$ were overlapped and then placed between two glass slides lined with Teflon sheets, submersed in CH_3CN and ultrasonicated for 1 h (0.5 sec pulse, 1 sec delay, 20% amplitude). Experiments were conducted under N_2 atmosphere at a heating rate of 3 °C/min and a frequency of 1 Hz. At 25 °C, the storage modulus is 25 ± 3 MPa.

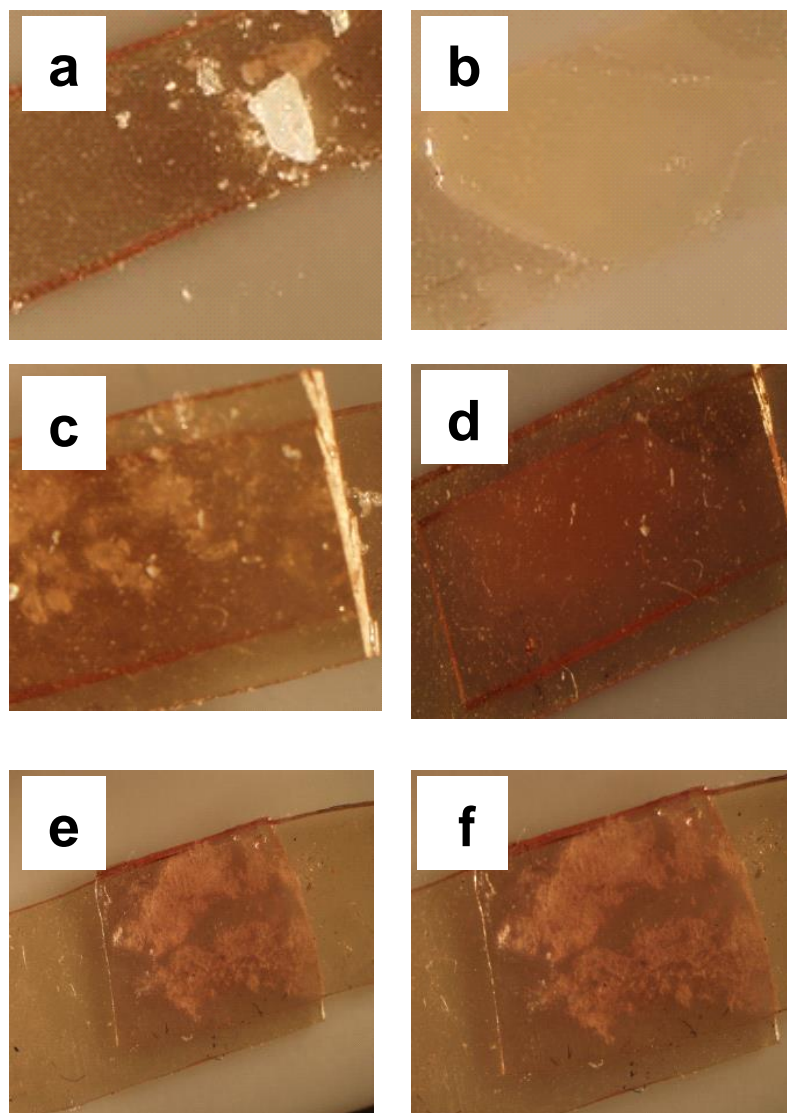


Figure S27. Temperature effects during welding by ultrasonication. Images of **a**, $[\text{Eu}(\text{BKB})_{1.5}](\text{ClO}_4)_3$ film covered with a low-melting crystalline compound (maleic anhydride, $T_m = 53\text{-}55\text{ }^\circ\text{C}$) shown at room temperature; **b**, $[\text{Eu}(\text{BKB})_{1.5}](\text{ClO}_4)_3$ film covered with maleic anhydride after heating for 3 h at $70\text{ }^\circ\text{C}$ in a vacuum oven; **c**, crystals of maleic anhydride sandwiched between two rectangular pieces of $[\text{Eu}(\text{BKB})_{1.5}](\text{ClO}_4)_3$ at room temperature; **d**, a sample as described in part **c** after heating for 3h at $70\text{ }^\circ\text{C}$ in a vacuum oven; the image shows that the maleic anhydride has melted under these conditions; **e**, a sample as described in part **c** after exposed to welding conditions (ultrasonication for 1 h); the image shows that the maleic anhydride has not melted under these conditions and that the $[\text{Eu}(\text{BKB})_{1.5}](\text{ClO}_4)_3$ films have been welded; **f**, the sample described in part **e**, but after 3 h of ultrasonication; the, image shows that the maleic anhydride has not melted under these conditions. The data show that the macroscopic temperature between the two polymer films during welding by ultrasonication remains below $55\text{ }^\circ\text{C}$ and that exposure to a temperature of $70\text{ }^\circ\text{C}$ does not lead to welding.

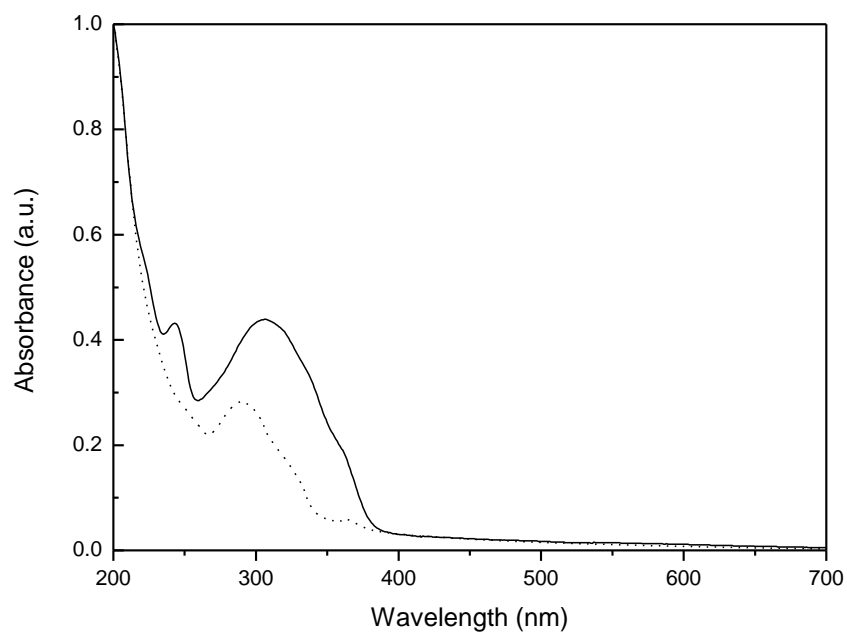


Figure S28. Solid-state UV-vis absorption spectra of the metallopolymers. UV-Vis absorption spectra acquired for drop-cast thin films from a CHCl_3 solution (0.8 mg/mL, 125 μL): $[\text{Eu}(\text{BKB})_{1.5}](\text{ClO}_4)_3$ (—, 3 μm thick) and $[\text{Eu}(\text{DKD})_{1.5}](\text{NH}_4\text{Et}_3)_3$ (⋯, 1.4 μm thick).

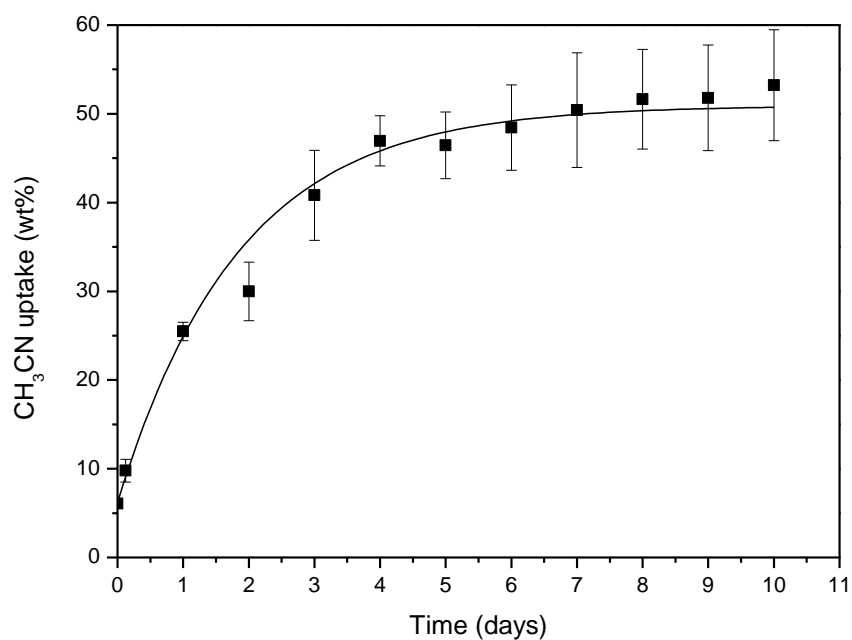


Figure S29. Swelling behavior of $[\text{Eu}(\text{BKB})_{1.5}](\text{ClO}_4)_3$. Thin films of $[\text{Eu}(\text{BKB})_{1.5}](\text{ClO}_4)_3$ were placed in CH_3CN for up to 10 days at room temperature. The degree of swelling was determined by measuring the weight of the samples pre- and post-swelling. Data points represent averages (number of individual measurements, $n = 3$) \pm standard deviation.

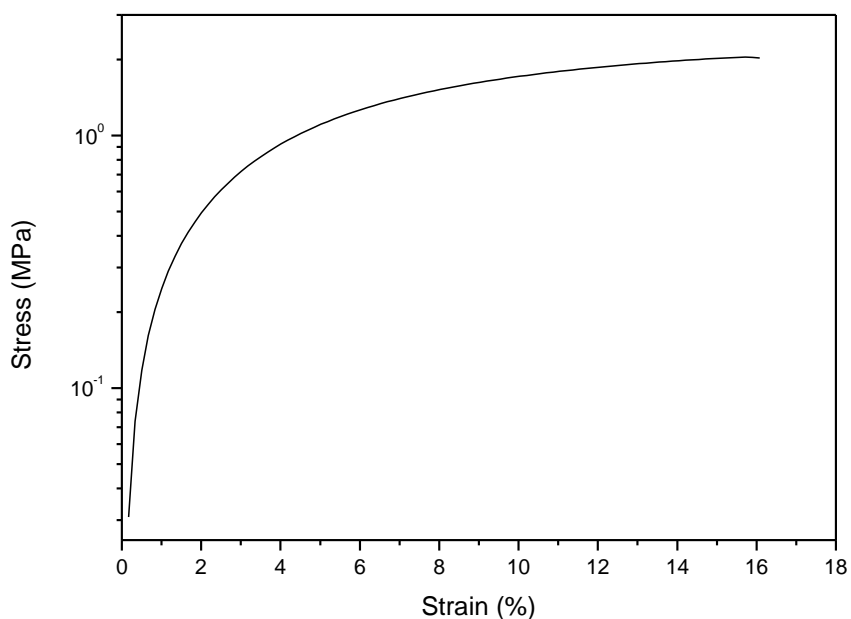


Figure S30. Mechanical analysis of solvent-swelled and re-dried $[\text{Eu}(\text{BKB})_{1.5}](\text{ClO}_4)_3$. Representative stress-strain curve of $[\text{Eu}(\text{BKB})_{1.5}](\text{ClO}_4)_3$ films that had been swollen in CH_3CN for 1 day and were subsequently dried overnight in vacuum at room temperature. Measurements were conducted under N_2 atmosphere at $25\text{ }^\circ\text{C}$, with a strain rate of $5\text{ \%}/\text{min}$. The mechanical data (average of $n=5$ samples) are as follows: stress and strain at break = 2.45 ± 0.47 and $15 \pm 4\text{ \%}$; Young's modulus = $27 \pm 5\text{ MPa}$; toughness = $25 \pm 4\text{ J/m}^3$.



Figure S31. Images of mechanically induced metal exchange in $[\text{Eu}(\text{BKB})_{1.5}](\text{ClO}_4)_3$ films. Thin films of $[\text{Eu}(\text{BKB})_{1.5}](\text{ClO}_4)_3$ were swollen in a solution of $\text{Fe}(\text{ClO}_4)_2$ in CH_3CN (10 mL, 0.5 mM) for 5 days. The films were then placed in CH_3CN and ultrasonicated for up to 1 h (0.5 sec pulse, 1 sec delay, 20% amplitude). Images of $[\text{Eu}(\text{BKB})_{1.5}](\text{ClO}_4)_3$ films before and after swelling in an $\text{Fe}(\text{ClO}_4)_2$ solution, and upon ultrasonication for 15, 30, 45, and 60 min are shown.

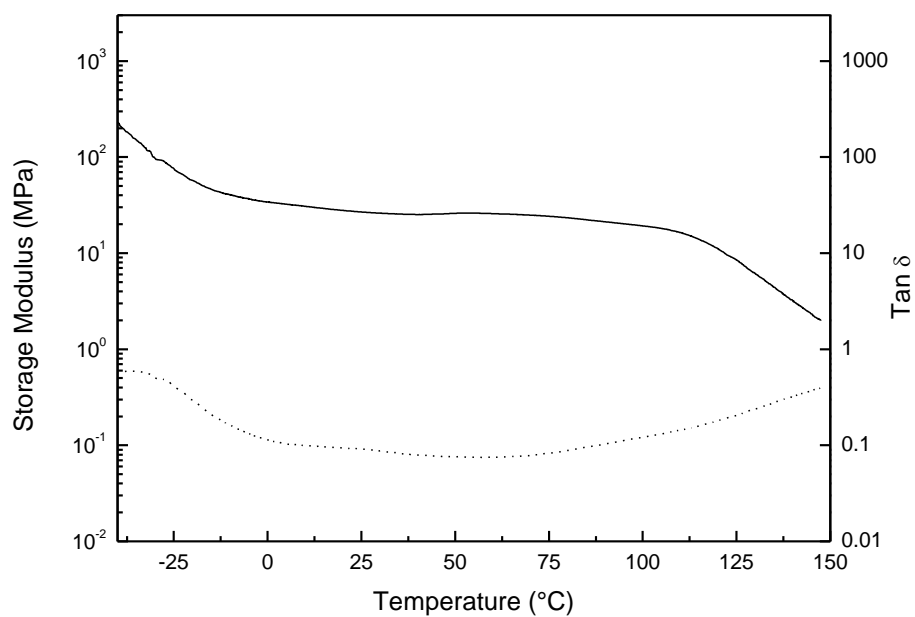


Figure S32. Mechanical analysis of $[\text{Fe}(\text{BKB})](\text{ClO}_4)_2$. Representative dynamic mechanical thermal analysis (DMTA) traces of $[\text{Fe}(\text{BKB})](\text{ClO}_4)_2$ (ca. 200 μm thickness) from -40 to 150 $^\circ\text{C}$; storage modulus (—) and $\tan \delta$ (···). Experiments were conducted under N_2 atmosphere at a heating rate of 3 $^\circ\text{C}/\text{min}$ and a frequency of 1 Hz. At 25 $^\circ\text{C}$, the storage modulus is 26 ± 1 MPa.

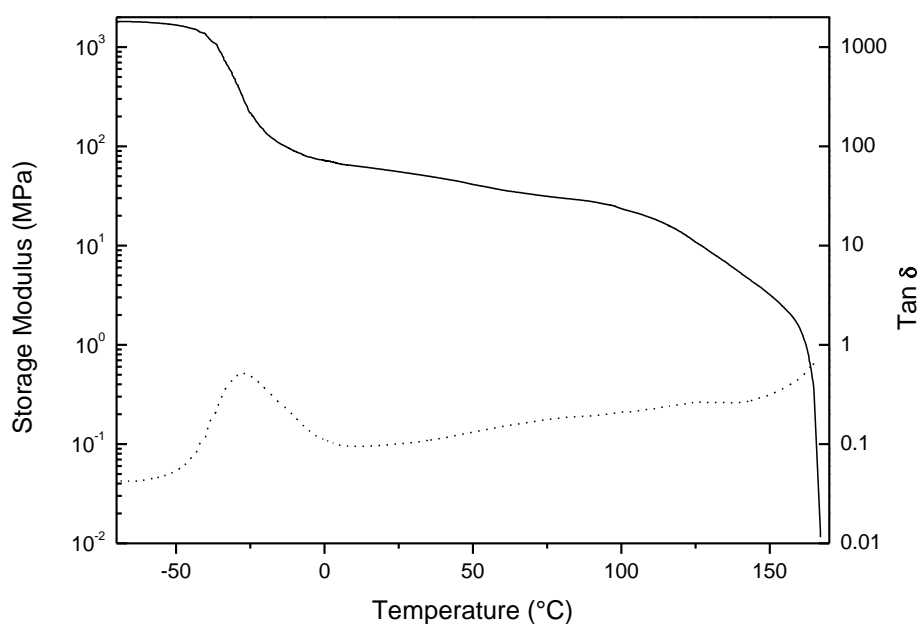


Figure S33. Mechanical analysis of $[\text{Eu}(\text{BKB})_{1.5}](\text{ClO}_4)_3$ after mechanically induced metal exchange. Representative dynamic mechanical thermal analysis (DMTA) traces $[\text{Eu}(\text{BKB})_{1.5}](\text{ClO}_4)_3$ imbided with Fe^{2+} from -70 to 160 °C storage modulus (—) and $\tan \delta$ (⋯). Thin films of $[\text{Eu}(\text{BKB})_{1.5}](\text{ClO}_4)_3$ were swollen in a solution of $\text{Fe}(\text{ClO}_4)_3$ in CH_3CN (10 mL, 0.5 mM) for 5 days. The films were then placed in CH_3CN and ultrasonicated for 1 h (0.5 sec pulse, 1 sec delay, 20% amplitude). Experiments were conducted under N_2 atmosphere at a heating rate of 3 °C/min and a frequency of 1 Hz.

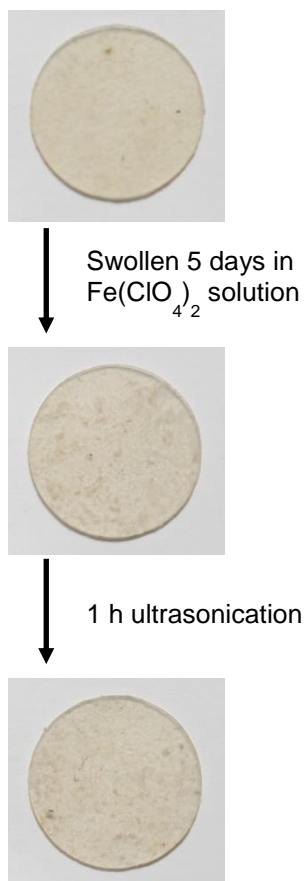


Figure S34. Images of $[\text{Eu}(\text{DKD})_{1.5}](\text{NHEt}_3)_3$ swollen and ultrasonicated in $\text{Fe}(\text{ClO}_4)_2$ solution. Thin films of $[\text{Eu}(\text{DKD})_{1.5}](\text{NHEt}_3)_3$ were swollen in a solution of $\text{Fe}(\text{ClO}_4)_2$ in CH_3CN (10 mL, 0.5 mM) for 5 days and then ultrasonicated in the same solution for 1 h (0.5 sec pulse, 1 sec delay).

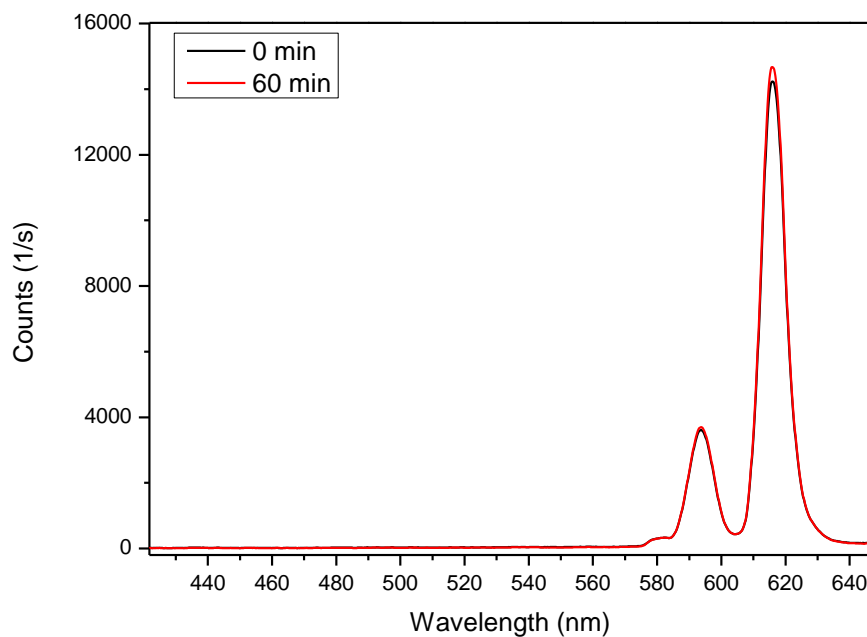


Figure S35. Photoluminescence spectra of [Eu(DKD)_{1.5}](NH₄Et₃)₃ polymer films. Thin films of [Eu(DKD)_{1.5}](NH₄Et₃)₃ were swollen in a solution of Fe(ClO₄)₂ in CH₃CN (10 mL, 0.5 mM) for 5 days and then ultrasonicated in the same solution for 1 h (0.5 sec pulse, 1 sec delay). The emission spectra were recorded before (black line) and after this process (red line) using a fiber optic cable and excitation with a handheld UV lamp ($\lambda = 254$ nm).

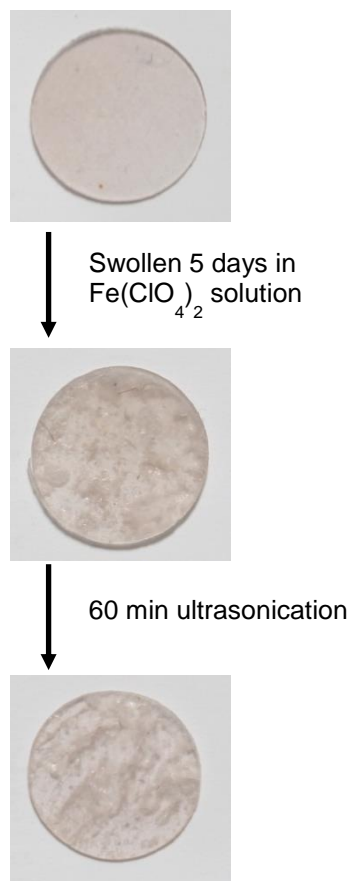


Figure S36. Images of $[\text{Zn}(\text{BKB})_{1.0}](\text{ClO}_4)_2$ swollen and ultrasonicated in $\text{Fe}(\text{ClO}_4)_2$ solution. Thin films of $[\text{Zn}(\text{BKB})_{1.0}](\text{ClO}_4)_2$ were swollen in a solution of $\text{Fe}(\text{ClO}_4)_2$ in CH_3CN (10 mL, 0.5 mM) for 5 days and then ultrasonicated in the same solution for 1 h (0.5 sec pulse, 1 sec delay).

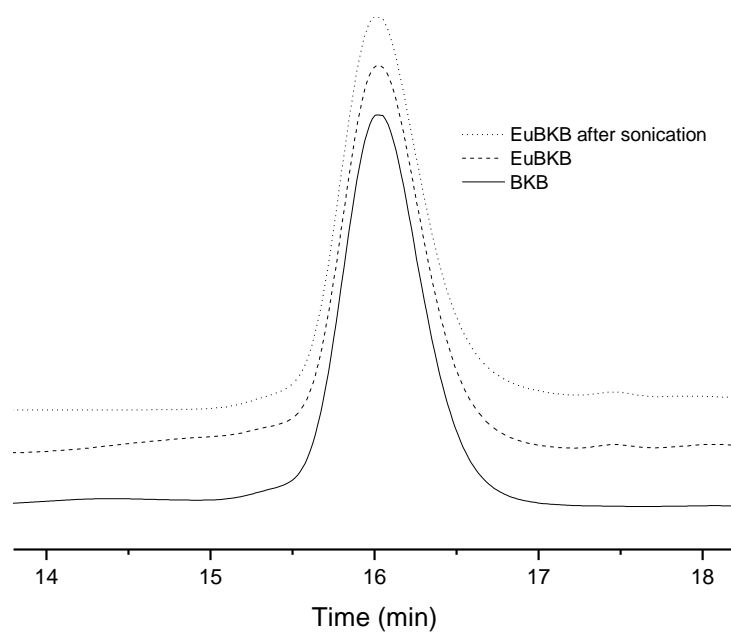


Figure S37. Gel permeation chromatography (GPC) traces of BKB and $[\text{Eu}(\text{BKB})_{1.5}](\text{ClO}_4)_3$ in THF. Samples of BKB (solid line) and $[\text{Eu}(\text{BKB})_{1.5}](\text{ClO}_4)_3$ (dash line) were analyzed by GPC before ultrasonication. Films of $[\text{Eu}(\text{BKB})_{1.5}](\text{ClO}_4)_3$ were ultrasonicated for 1 h (0.5 sec pulse, 1 sec delay) and then dried in vacuum. Ultrasonicated $[\text{Eu}(\text{BKB})_{1.5}](\text{ClO}_4)_3$ films (dotted line) were then dissolved in THF and analyzed by GPC.

6. Characterization of compounds

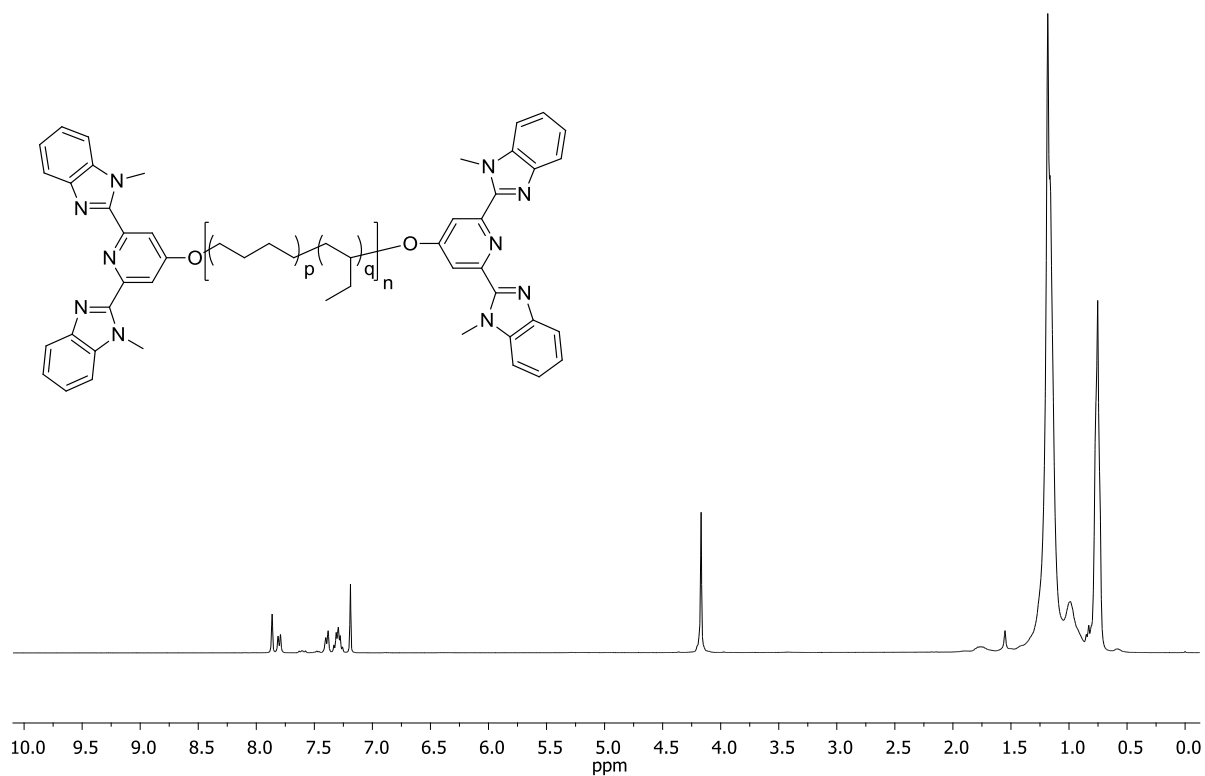


Figure S38. ¹H NMR spectrum of the BKB macromonomer. ¹H NMR (360 MHz, CDCl₃): δ 7.93 (s, 4H), 7.86 (d, *J* = 7.8 Hz, 4H), 7.45 (d, *J* = 7.8 Hz, 4H), 7.37 (m, 8H), 4.24 (broad s, 16H), 1.25 (m, 437 H), 0.82 (m, 152H).

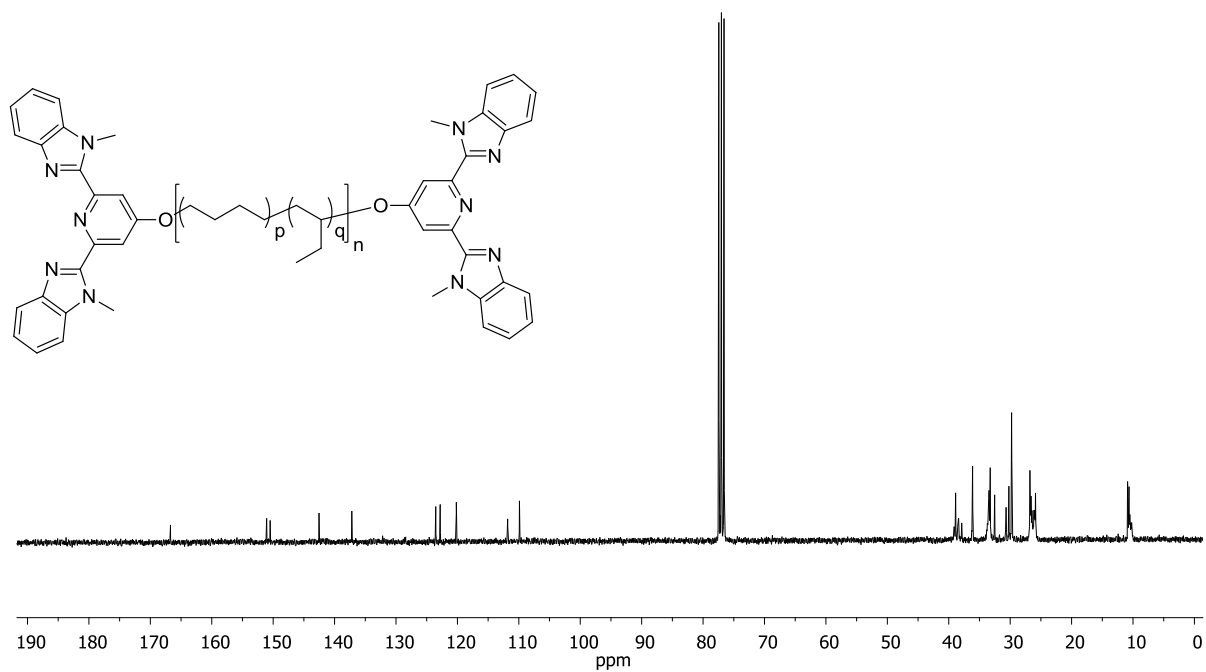


Figure S39. ^{13}C NMR spectrum of the BKB macromonomer. ^{13}C NMR (75 MHz, CDCl_3): δ 166.59, 151.27, 150.31, 142.64, 137.20, 123.63, 122.89, 120.17, 112.05, 109.82, 68.56, 38.40-37.83, 35.96, 33.49, 33.24, 32.53, 30.66, 30.21, 29.77, 26.78-25.88, 10.83-10.18.

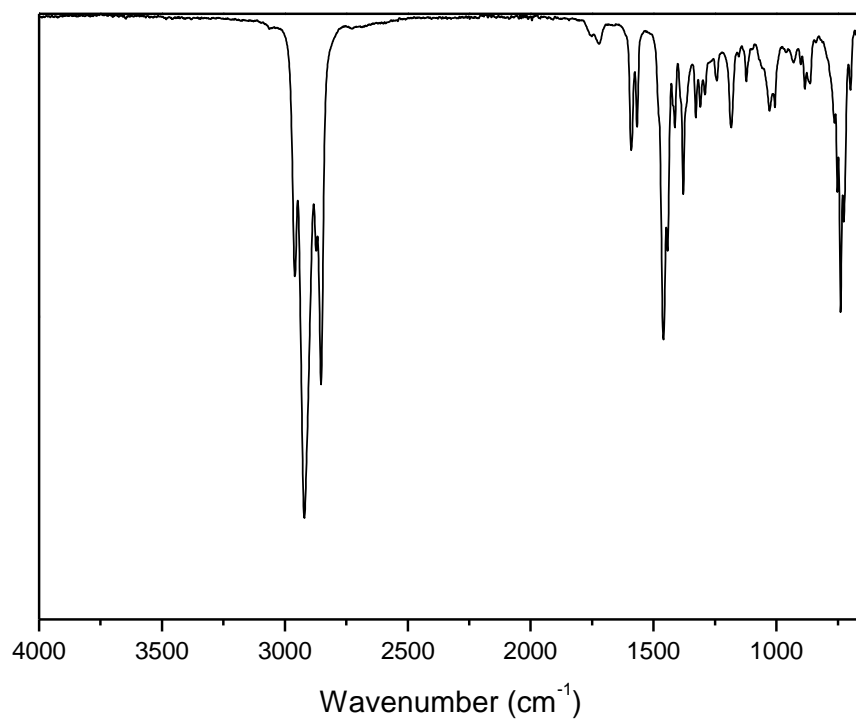


Figure S40. FT-IR spectrum of the BKB macromonomer. IR (cm^{-1}) 2959, 2920, 2872, 2852, 1722, 1591, 1567, 1459, 1443, 1413, 1379, 1328, 1309, 1290, 1242, 1184, 1122, 1028, 1006, 930, 884, 863, 763, 752, 738, 726, 698, 643, 621.

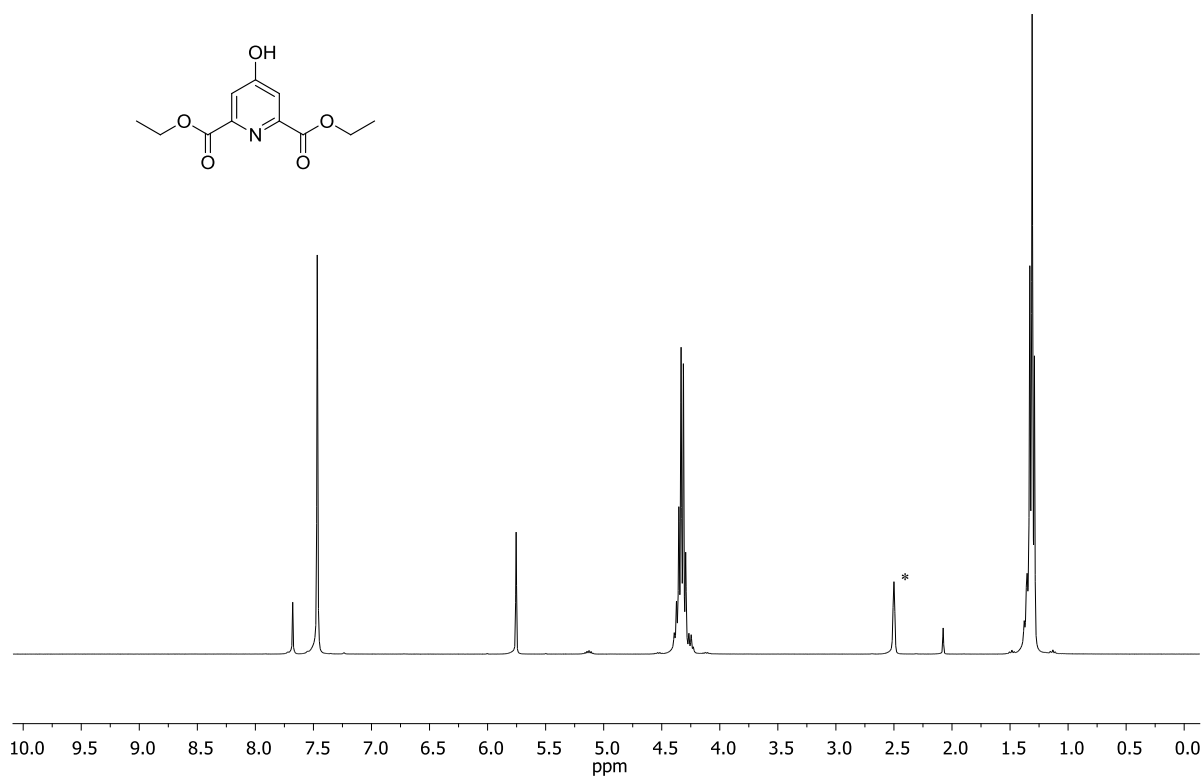


Figure S41. ¹H NMR spectrum of 4-hydroxy-pyridine-2,6-dicarboxylic acid diethyl ester. ¹H NMR (360 MHz, DMSO-*d*₆) δ 7.47 (s, 2H, Ph-*H*), 5.75 (s, 1H, C-*OH*), 4.32 (q, *J* = 7.1 Hz, 4H, -O-*CH*₂-*CH*₃), 1.31 (t, *J* = 7.2 Hz, 6H, -O-*CH*₂-*CH*₃).

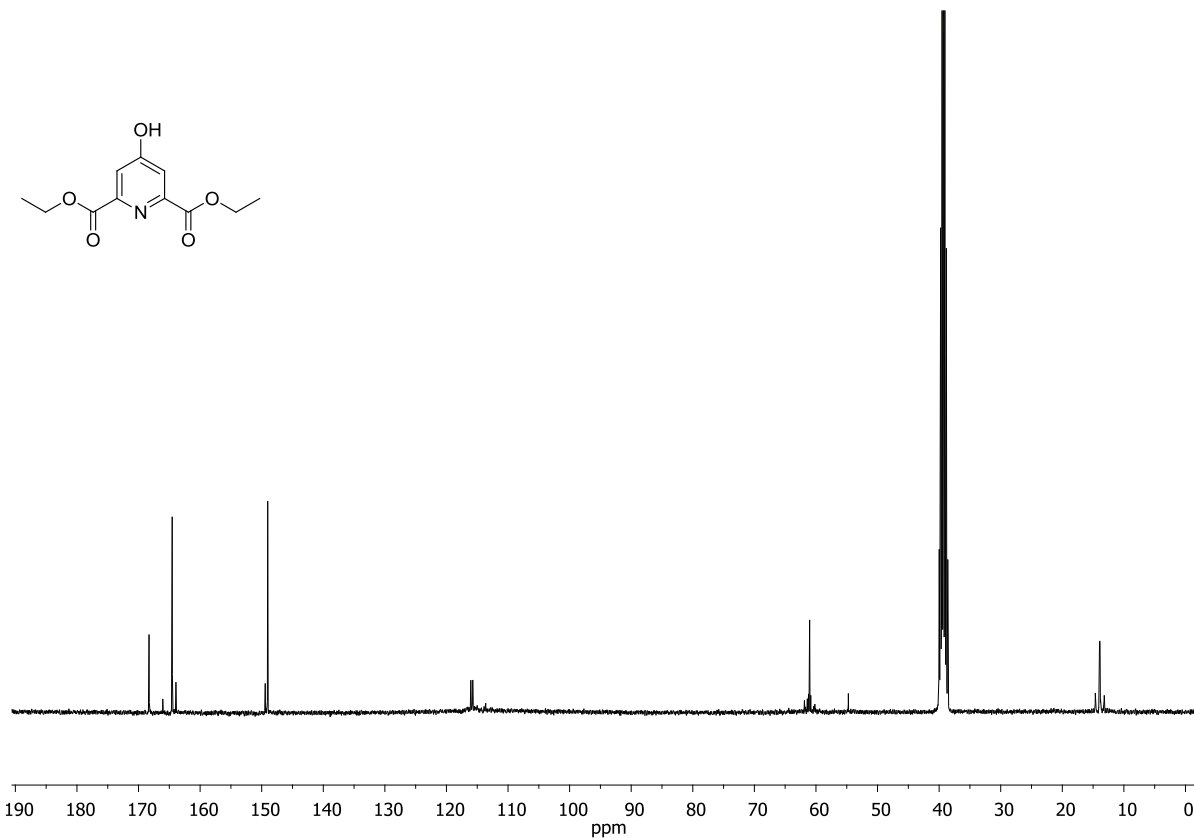
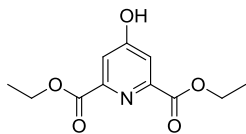


Figure S42. ^{13}C NMR spectrum of 4-hydroxy-pyridine-2,6-dicarboxylic acid diethyl ester. ^{13}C NMR (90 MHz, $\text{DMSO-}d_6$) δ 168.85, 165.08, 149.57, 116.60, 116.28, 61.58, 14.50, 14.42.

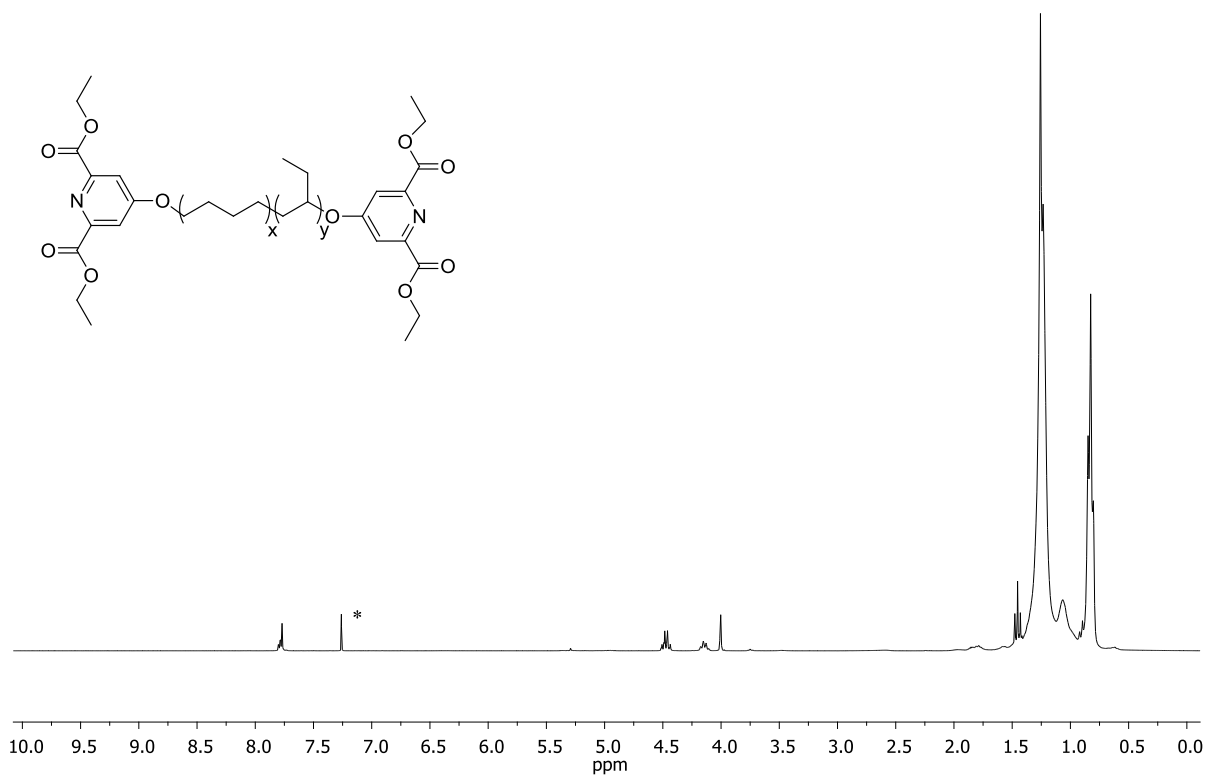


Figure S43. ¹H NMR spectrum of the ethyl protected DKD macromonomer. ¹H-NMR (CDCl₃, 300 MHz) δ 7.79 (s, 4H), 4.49 (q, 5H), 4.16 (q, *J* = 6.8 Hz, 4H), 4.02 (s), 1.93 – 0.96 (m, 510H), 1.47 (t, *J* = 7.1 Hz, 7H), 0.84 (t, *J* = 6.8 Hz, 157H). Small impurities at 4.02 ppm originating from DIAD, and partial deprotection of carboxylic acid were observed.

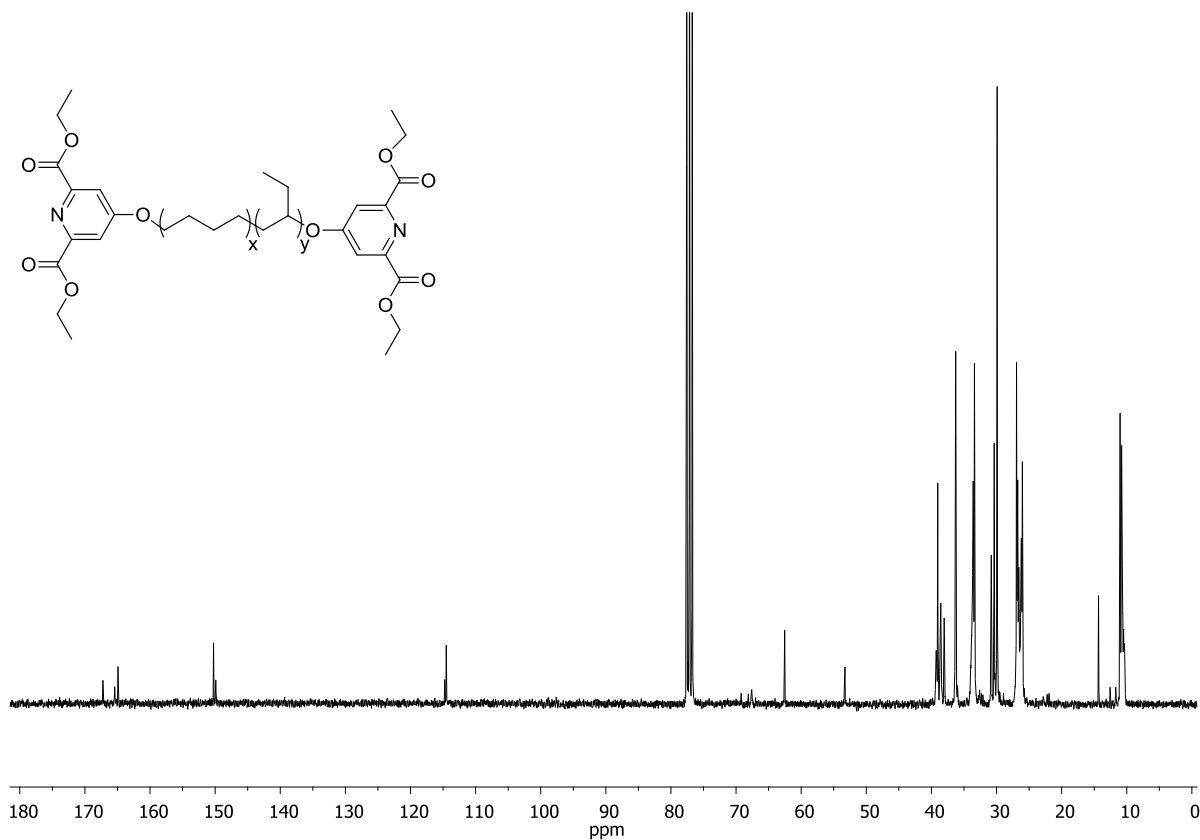


Figure S44. ^{13}C NMR spectrum of the ethyl protected DKD macromonomer. ^{13}C NMR (CDCl_3 , 90 MHz) δ 167.09, 165.28, 164.77, 150.10, 149.75, 114.60, 114.49, 114.36, 62.38, 53.12, 39.10, 38.87, 38.40, 37.89, 36.12, 33.44, 33.24, 30.66, 30.21, 29.75, 26.78, 26.60, 26.44, 26.26, 26.13, 26.04, 25.88, 14.19, 10.88, 10.68, 10.64, 10.53, 10.35, 10.21.

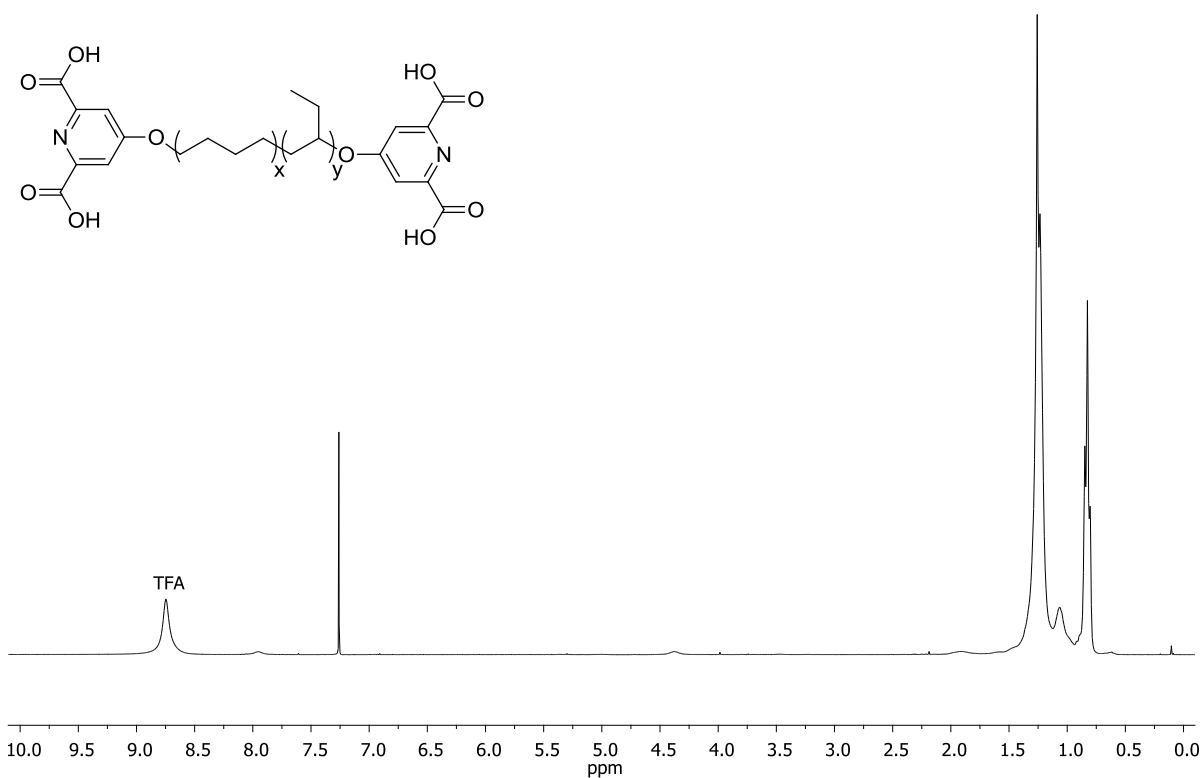


Figure S45. ¹H NMR spectrum of the DKD macromonomer. ¹H-NMR (CDCl₃/TFA (30:1), 300 MHz): δ 8.00 (s, 4H), 4.42 (s, 4H), 2.22 – 0.97 (m, 561H), 0.83 (t, *J* = 6.8 Hz, 180H).

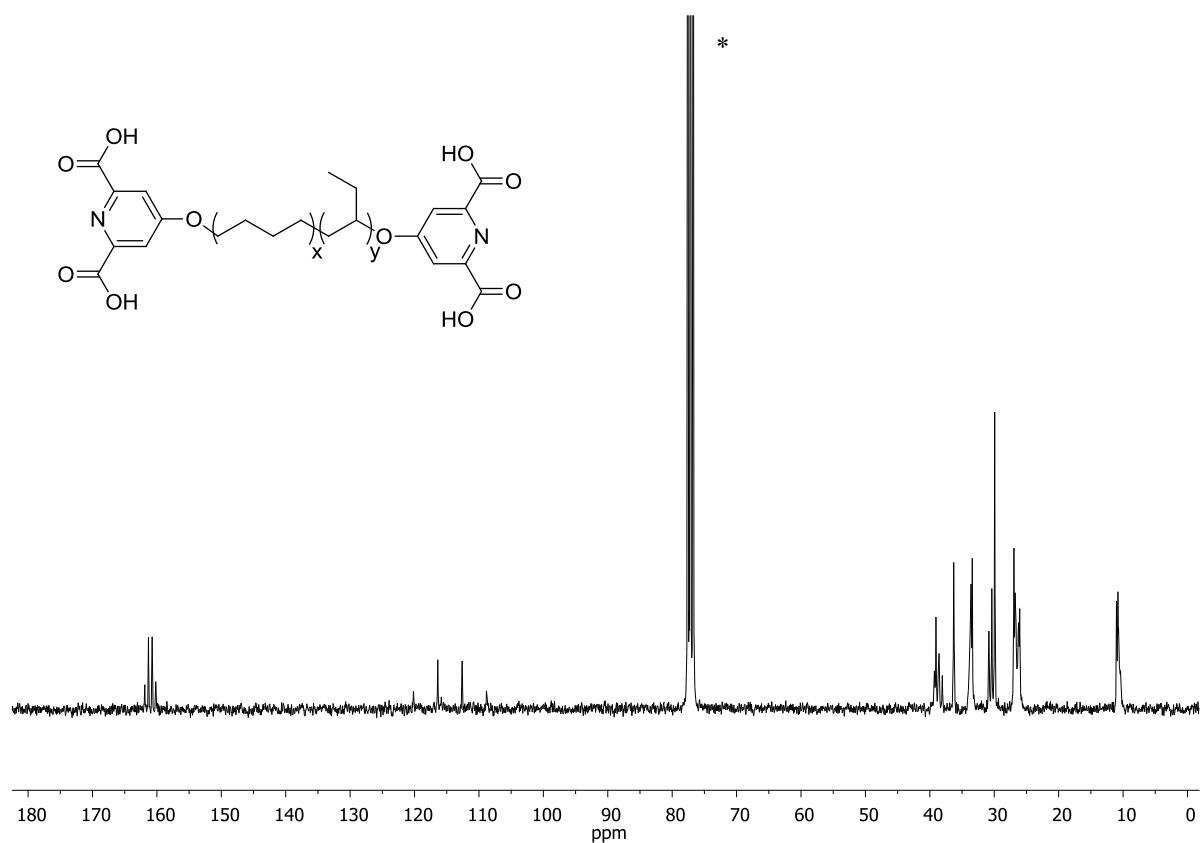


Figure S46. ^{13}C NMR spectrum of the DKD macromonomer. ^{13}C NMR (75 MHz, CDCl_3) δ 77.16, 39.05, 36.29, 33.61, 33.41, 30.83, 30.38, 29.93, 26.95, 26.76, 26.61, 26.29, 26.21, 26.05, 11.02, 10.80.

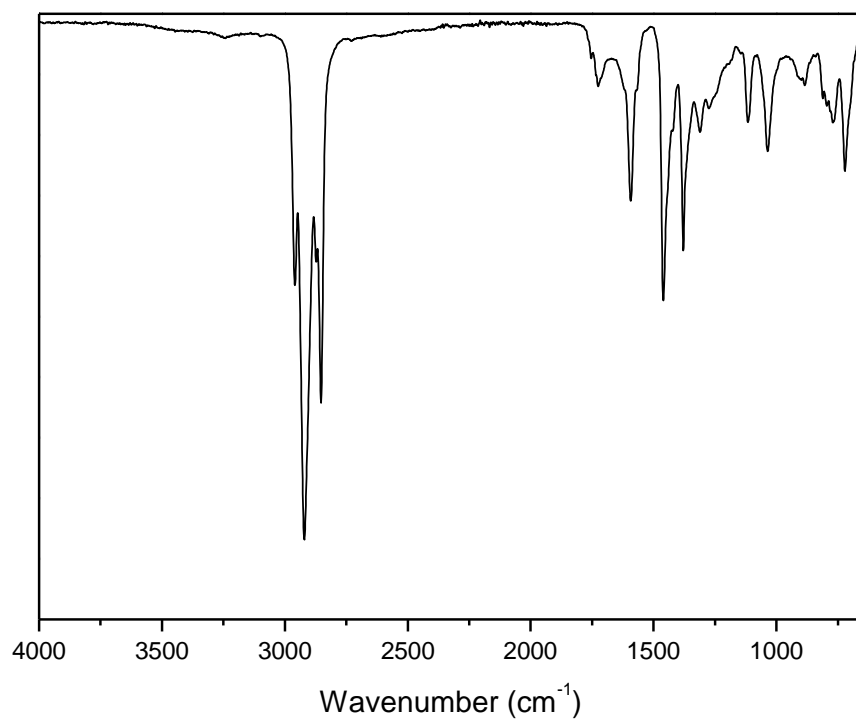


Figure S47. FT-IR spectrum of the DKD macromonomer. IR (cm⁻¹) 2959, 2920, 2872, 2852, 1725, 1592, 1460, 1378, 1310, 1274, 1116, 1035, 884, 770, 721, 637.

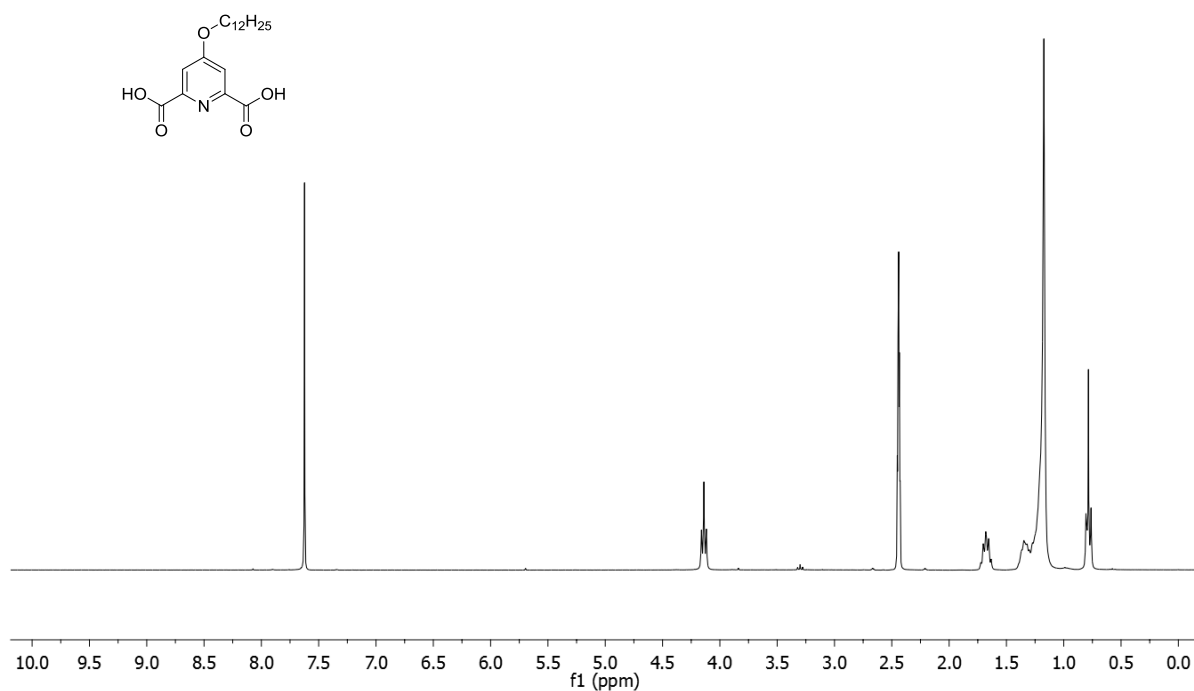


Figure S48. ¹H NMR spectrum of diethyl 4-(dodecyloxy)pyridine-2,6-dicarboxylate (dpaC₁₂H₂₅). ¹H NMR (300 MHz, DMSO-*d*₆) δ 7.62 (s, 2H, Ph-*H*), 4.14 (t, *J* = 6.4 Hz, 2H, -O-CH₂-(CH₂)₁₀-), 1.77 – 1.55 (m, 2H, -O-CH₂-CH₂-), 1.45 – 1.30 (m, 2H, -O-(CH₂)₂-CH₂-), 1.22 (m, 20H, -(CH₂)₁₀-CH₃), 0.78 (t, *J* = 6.7 Hz, 3H, -CH₂-CH₃).

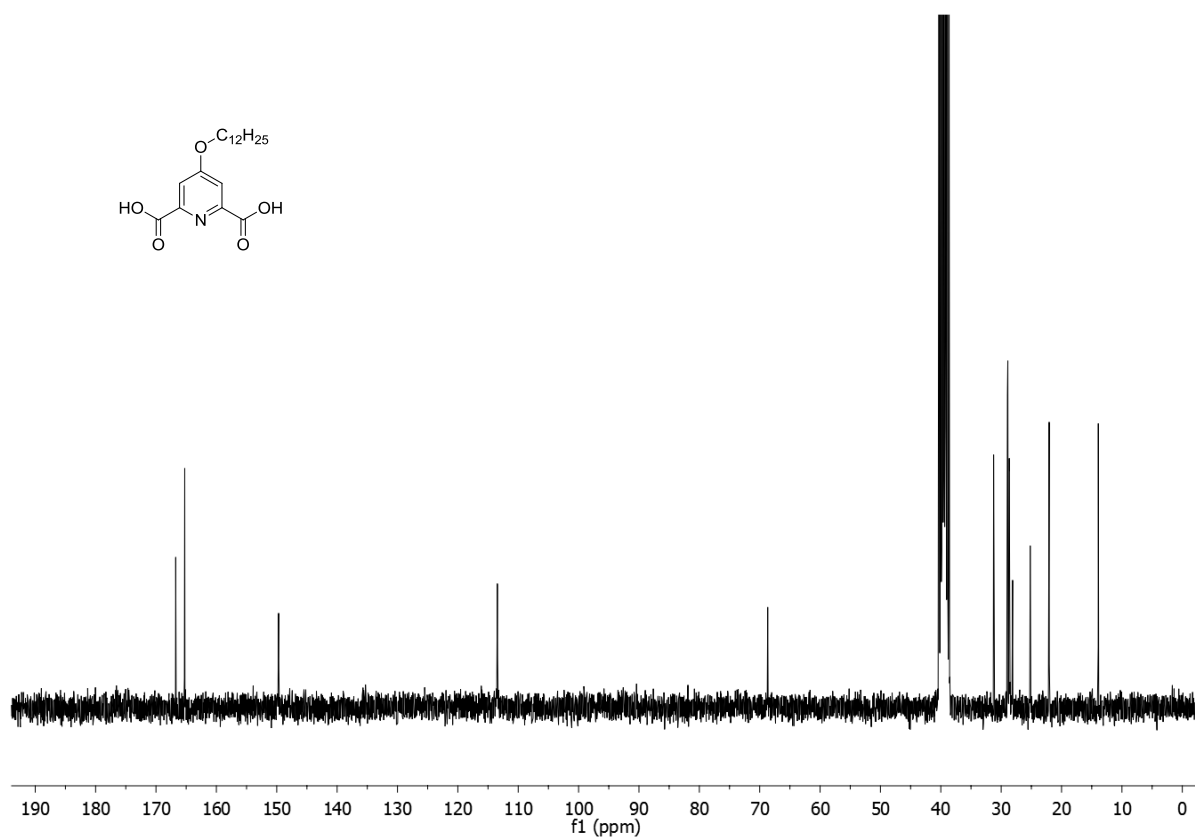


Figure S49. ¹³C NMR spectrum of diethyl 4-(dodecyloxy)pyridine-2,6-dicarboxylate (dpaC₁₂H₂₅). ¹³C NMR (75 MHz, DMSO-*d*₆) δ 166.73, 165.24, 149.69, 113.45, 68.67, 31.25, 28.98, 28.96, 28.90, 28.66, 28.58, 28.11, 25.19, 22.05, 13.91.

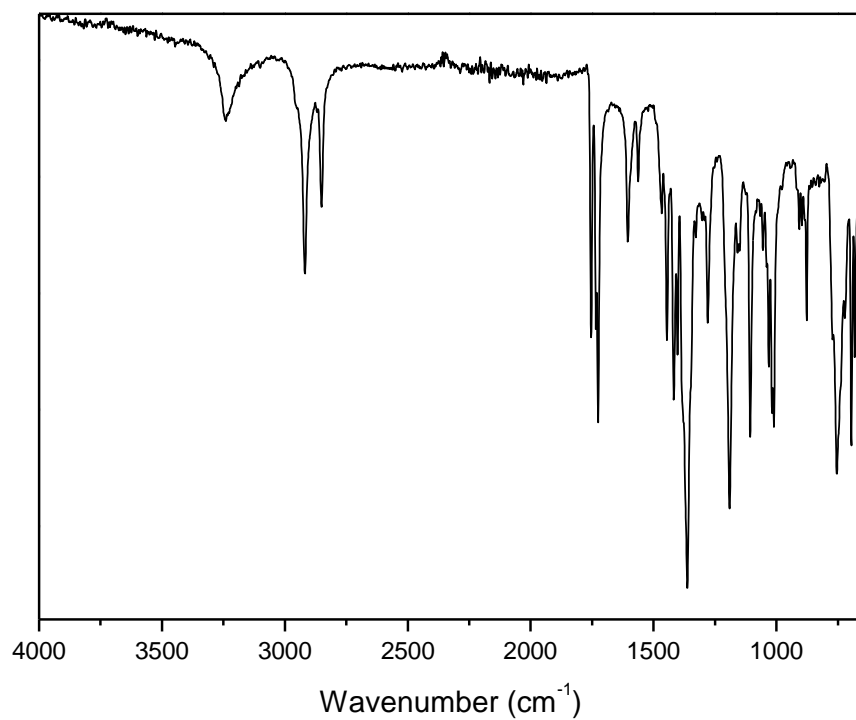


Figure S50. FT-IR spectrum of diethyl 4-(dodecyloxy)pyridine-2,6-dicarboxylate (dpaC₁₂H₂₅). IR (cm⁻¹) 3240, 2918, 2850, 1753, 1734, 1725, 1604, 1562, 1466, 1445, 1417, 1402, 1362, 12791, 1190, 1106, 1055, 1031, 1010, 907, 877, 754, 695, 681, 639, 614.

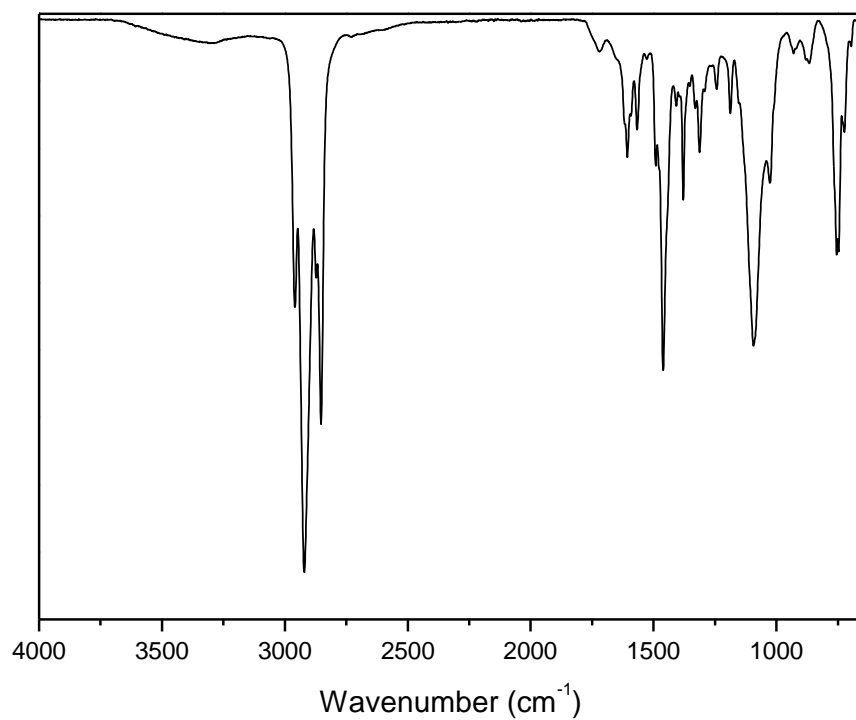


Figure S51. FT-IR spectrum of metallosupramolecular polymer [Eu(BKB)_{1.5}](ClO₄)₃. IR (cm⁻¹) 3309, 2959, 2921, 2872, 2852, 1719, 1606, 1566, 1491, 1460, 1407, 1379, 1330, 1312, 1243, 1187, 1093, 1026, 930, 866, 754, 747, 723, 622.

7. Mechanical properties

Table S1. Mechanical properties of films of [Eu(BKB)_{1.5}](ClO₄)₃ (with different treatments), [Eu(DKD)_{1.5}](NHEt₃)₃ and [Fe(BKB)](ClO₄)₂.

Samples	Storage Modulus (MPa)^a	Maximum Stress (MPa)^b	Stress at Break (MPa)^b	Strain at Break (%)^b	Young's Modulus (MPa)^b	Toughness 10⁴ (J/m³)^b
[Eu(BKB) _{1.5} ^c](ClO ₄) ₃ Original	23 ± 6	2.0 ± 0.7	1.6 ± 0.2	17 ± 3	24 ± 5	20 ± 2
[Eu(BKB) _{1.5} ^d](ClO ₄) ₃ Cut and welded	25 ± 3	2.1 ± 0.9	1.6 ± 0.7	14 ± 4	37 ± 8	20 ± 6
[Eu(BKB) _{1.5}](ClO ₄) ₃ Swollen and dried	25 ± 3	2.5 ± 0.5	2.5 ± 0.4	15 ± 4	27 ± 5	25 ± 4
[Eu(BKB) _{1.5}](ClO ₄) ₃ Fe ²⁺ -imbibed and sonicated	n.a.	1.3 ± 0.3	7.0 ± 2.0	7 ± 2	21 ± 6	5 ± 1
[Eu(DKD) _{1.5} ^e](NHEt ₃) ₃ Original	8 ± 2	1.2 ± 0.4	1.0 ± 0.1	11 ± 0	16 ± 6	7 ± 2
[Fe(BKB)](ClO ₄) ₂ Original ^e	26 ± 1	1.2 ± 0.9	0.9 ± 0.5	12 ± 4	20 ± 5	17 ± 3

^aMeasured by DMTA at 25 °C. ^bMeasured by stress-strain experiments. ^cOriginal indicates the original film after compression molding. ^dHealed indicates dog bone samples mended after being cut, overlapped, and welded together. Data represent averages of n = 5 individual measurements except ^en = 3 ± standard deviation. Toughness was calculated by integration of the area under the stress strain curves.

8. Supporting movie

Movie M1. Mechanically induced dissociation of metallosupramolecular polymers. Shown are two cuvettes containing solutions of $[\text{Eu}(\text{BKB})_{1.5}](\text{ClO}_4)_3$ in CHCl_3 (2 mg/mL) under UV illumination ($\lambda = 365$ nm). A ultrasonic horn sonicator equipped with a tapered microtip (1/8 in) was placed into one of the cuvettes (left) and the other cuvette was used as a reference (right). The $[\text{Eu}(\text{BKB})_{1.5}](\text{ClO}_4)_3$ solution was ultrasonicated for 20 sec (30% amplitude) and then left to stand, demonstrating the reversibility and mechano-responsive behavior of metallosupramolecular polymers.